Estimation of the Local Seismic Amplification on an Industrialized Site in the French Rhône Valley

C. Gélis, Lena Cauchie, E.M. Cushing, Berenice Froment, Sylvain Franco, Hervé Jomard, Denis Moiriat, Ludmila Provost, Begum Sariguzel, Haifa Tebib

Estimation of the local seismic amplification on an industrialized site in the French Rhône Valley

C. Gélis[1], L. Cauchie[1,2], E.M. Cushing[1], B. Froment[1], S. Franco[1,3], H. Jomard[1], D. Moiriat[1], L. Provost[1], B. Sariguzel[1], H. Tebib[1,4]

1 : IRSN, France

2 : now at University of Liege, Belgium

3 : now at Ginger CEBTP, France

4 : now at University of Strathclyde, Glasgow, UK

Abstract

The so-called site effects caused by superficial geological layers may be responsible for strong ground motion amplification in certain configurations. We focus here on the industrialized Tricastin area, in the French Rhône valley, where a nuclear site is located. This area lies above an ancient Rhône Canyon whose lithology and geometry make it prone to site effects. This study presents preliminary measurements to investigate the local seismic amplification. We deployed 3 seismic stations in the area for several months: two stations were located above the canyon, the third one was located on a nearby reference rock site. The recorded seismicity was analysed using the Standard Spectral Ratio technique (SSR). The estimated amplification from weak motions reaches a value of 6 for some frequencies. These first results confirm the possibility of estimating seismic amplification using earthquakes recorded for less than one year, in this highly anthropogenic and industrialized environment, despite the local low-to-moderate level of seismicity. Noise-based SSR, that presents an obvious interest in such seismic context, shows also promising results in the area. To complement this empirical approach, we estimated the amplification using 1D wave propagation modelling. This numerical estimate is based on shear wave velocity profiles resulting from geophysical characterization campaigns. Comparison of the two approaches at low frequency, where numerical estimate is considered as the most representative, tends to suggest that edge-generated surface waves may have a strong influence in the local seismic response. This interpretation will be further investigated in the future.

Keywords : site effects ; seismic ground motion amplification ; Messinian canyon ; Surface Waves Dispersion Analysis

Introduction

As it is well known, superficial geological layers can strongly modify the surface ground motion induced by an earthquake. These so-called site effects are responsible for strong ground motion amplification in certain geological configurations, such as sedimentary basins. In these structures, the impedance contrast between the geological layers filling the basin and the bedrock at the basement, together with the basin shape may be both responsible for ground motion amplification and complex wave propagation inside the basin (e.g., Semblat et al., 2005; Semblat et al., 2000). Depending on the

basin characteristics, local 1D resonance, edge-generated waves traveling across the basin, constructive or destructive interferences and 2D/3D resonance can take place (Bard and Bouchon, 1985; Kawase, 1996; Roten et al., 2006; Bindi et al., 2009; Ktenidou et al., 2016).

In this paper we focus on the Tricastin area, in the Rhône valley (South-East France), where the Tricastin Nuclear Site (TNS) is located. TNS consists of a power plant and a collection of nuclear fuel cycle facilities. TNS is located above an ancient Rhône canyon. This canyon was dug following the closure of the Gilbraltar strait (5.95-5.32 Ma) and the resulting fall of the Mediterranean Sea level during the Messinian time. The fall reached -1500 m in some areas leading to the incision of Messinian Canyons such as the Rhône Canyon (Clauzon, 1982; Suc et al., 2011). After the reopening of the Gibraltar strait, the canyon was flooded and then filled with Pliocene and Quaternary sediments (sands and marls). The Rhône Messinian canyon can be locally very deeply incised in Cretaceous sandstones and limestones. Given this geological configuration, the area is prone to site effects. Such effects must be estimated and taken into account for seismic hazard assessment. Depending on the location of nuclear installations, IRSN as the French Technical Safety Organisation (TSO) may be led to conduct studies on this topic.

The Tricastin region is characterized by a low-to-moderate seismicity. The last important earthquake in the area is the Mw 4.9 Le Teil earthquake (2019, November 11th) that took place about 20 km northward and severely damaged several villages in the vicinity of the rupture area (Ritz et al., 2020; Cornou et al., 2021; Delouis et al., 2021). Before this event, seismic swarms occurred in 1773, 1872-1874, 1934-1936 and 2002-2003 in the Tricastin region (Bollinger et al., 2021). Significant damages were reported in villages during seismic swarms in 1773 and 1872-1874, as documented in the SisFrance database of historical earthquakes (http://www.sisfrance.net, Jomard et al., 2021). The 2002-2003 swarm was recorded by a local seismicity network (Thouvenot et al., 2009). More details about seismicity is the Tricastin region can be found in the Supplementary Material.

This study presents preliminary measurements to investigate the potential of the canyon to generate ground motion amplification in the area of Tricastin. In particular, our aim is to assess if it is possible to acquire some observations that could be useful for characterizing the site effects in this industrialized and anthropogenic area located in a low-to-moderate seismicity region.

In this context, we installed 3 seismic stations in the area of Tricastin for several months. Two stations were located above the Rhône Messinian canyon, the third one was located on nearby Cretaceous outcrop (considered as a reference site, that is, free of amplification effect). These stations have been deployed for durations ranging from 6 months to 1 year in order to record the seismicity. The data were analysed to extract information regarding the amplification related to the presence of the canyon. In particular, the so-called Standard Spectral Ratios (SSR, Borcherdt, 1970) are applied between recordings at the different stations. To complement this empirical approach, we examined the amplification estimated using a 1D numerical approach. This numerical estimate is based on 1D shear wave velocity (Vs) profiles obtained at 2 of the stations resulting from geophysical site characterization campaigns. After having introduced the local geology of the Messinian Canyon (Section 1), we will present the criteria for the choice of the location of the 3 stations (Section 2). Section 3 is devoted to the analysis of the seismic data acquired. In addition to the analysis performed on earthquake recordings, preliminary tests on seismic ambient noise are also shown. Section 4 is devoted to the 1D numerical estimation, by respectively presenting the determination of the two local 1D Vs profiles and the numerical computation of the amplification. In Section 5, we will then compare the 1D numerical estimate of seismic amplification with the empirical one at low frequency and we will discuss possible interpretations in terms of physical processes related to site effects.

1. Local geology of the Messinian canyon

The geology, location and depth of the Messinian canyon remains poorly documented in the Tricastin area. Early studies report some structural interpretations (Denizot, 1952; Ballesio, 1972; Mandier, 1984) and explain the digging of the canyon by crustal vertical movements. Moreover, they propose some sections crossing Pliocene series, placing a fault to explain the local thickening of Pliocene series. On the contrary, Clauzon (1982) is the first author to assert that the messinien rhodanian talweg longitudinal profile (based on borehole analysis all along the river course) is the result of regressive erosion associated to the falling of the Mediterranean base level. In the studied area, some boreholes reach at least the Pliocene (mostly the easily identifiable marine Piacenzian blue marls). The two deep boreholes located southeast of Pierrelatte (DPG1) and along the Donzère Canal at Saint-Paul-Trois-Châteaux (F1) reach infra Pliocene basement, thereby bringing information about the canyon depth and its filling in the eastern part of the Tricastin valley (Fig. 1). The DPG1 borehole was dug in 1959 down to 351 m depth. The F1 borehole was dug in 2003 down to 834 m in the Messinian canyon and the Cretaceous series below. They both show a thick Pliocene series filling a canyon incised in cretaceous series (upper Aptian clayey marls – locally named Gargasian- overlying Barremian hard and massive reef crystalline limestones – locally named Urgonian). From F1, the depth of the canyon at the latitude of Saint-Paul-Trois-Châteaux is estimated to be at least 460 m. In the DPG1 borehole located 4 km northward, the borehole reaches the canyon bottom at 291 m depth. This is much shallower than in F1, meaning that the DPG1 borehole is located above the canyon rim. The canyon axis may be estimated from the above mentioned boreholes and other data such as specific studies for the TGV fast train (Mocochain et al., 2006) that evidenced the canyon position at the Malataverne Pass (Figs 1 and 2). Other boreholes data and geological maps help to approximately locate the canyon rims (Fig. 1). Some particular shallow Cretaceous coring or outcrops show the existence of “Islands” in between the canyon in Pierrelatte town where a Cretaceous rock is visible and, in the area located 4 km west of Bollène where some boreholes reach upper cretaceous sandstones and lignite at low depth (Preference borehole location on Figure 1). From the last observation, the width of the canyon at the latitude of Bollène cannot be greater than 4 km.

2. Criteria used to select the location of measurement sites

In this section, we present criteria for selecting seismic station locations in the Tricastin area. Two stations are located above the canyon sedimentary filling, the third station lies on cretaceous outcrop (Urgonian limestones), considered here as a reference site, that is free of amplification caused by the canyon. We based our choice first on geological investigations (field survey and borehole database analysis) or Geophysical Noise Horizontal-to-Vertical Spectral Ratio (NHVSR, Nakamura, 1989) measurements are then computed to confirm the geological choice.

The first site on the canyon filling is chosen nearby the deep borehole F1 (see Fig. 1) at approximately 4 km from the ADHE reference. The proximity of this site to this borehole is a key criterion for our experiment since the knowledge of the geological log will help interpreting seismic observations. This site is named PAUL in reference to the town of Saint-Paul-Trois-Châteaux where it is located. NHVSR measurements were carried out to assess the fundamental resonance frequency of this site. The results are presented hereafter. Given the industrial and anthropogenic environment nearby, this site does not allow for further characterization investigations such as SWDA (Surface Waves Dispersion Analysis) that require measurements over an extended area.

For this reason, a second site (BOLL) was chosen further south (i.e. downstream of the first point at approximately 5.2 km from the BOLL site and 7 km from the ADHE site, with the 3 stations roughly aligned), in the town of Bollène. BOLL is located above the assumed path of the canyon as discussed in section 1 and suggested by Mocochain et al. (2009). This site, being surrounded by farm fields, makes array-based SWDA possible, such as the AVA (Ambient Vibration Array) method. Both NHVSR and AVA experiments were thus conducted at this site to characterize the resonance frequency and 1D Vs profiles that will be presented in section 4a.

In order to characterize the amplification of the seismic signal at BOLL and PAUL sites due to the canyon and its filling, we targeted a reference station located on a rock representative of the regional substratum of the Rhone valley. As discussed in section 1 the reference rock is the Urgonian limestone. After a field survey, we chose a limestone massif located south of the La Garde-Adhémar village. At this site named ADHE, limestones are outcropping, free of alteration and soil cover, and show a very slight dip towards the southeast. These characteristics are considered as good criteria for the location of the reference station. In addition, the distance to BOLL and PAUL sites is adapted to compute amplification using regional earthquakes. At this site, NHVSR and SWDA measurements were also performed.

For sake of simplicity, in the following we will use the term “sediment station/site” (resp. “rock/reference station/site”) to refer to a station/site located above the canyon sedimentary filling (resp. Cretaceaous outcrop).

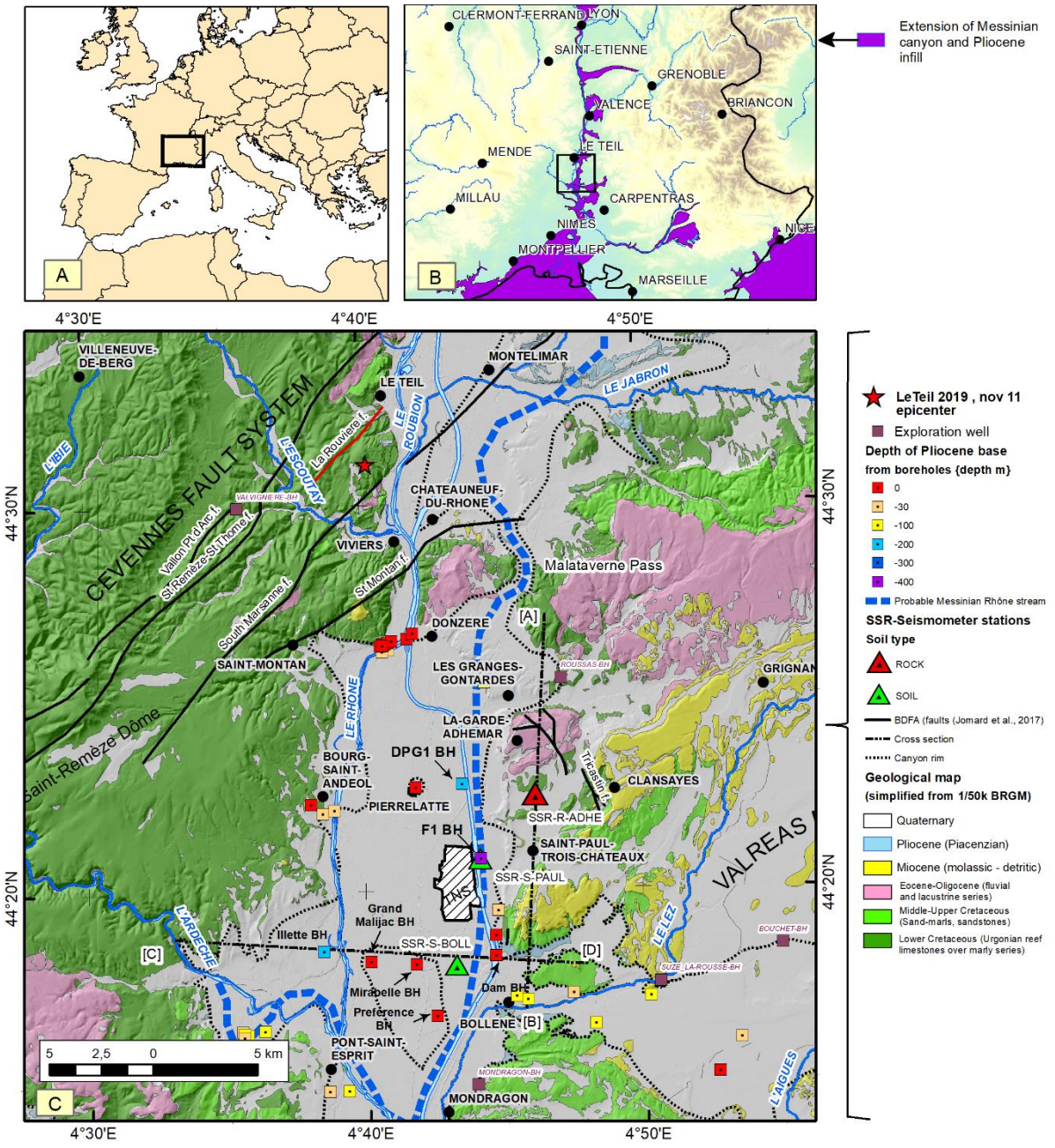

FIGURE 1: geological map at local scale with locations of SSR stations (coloured triangles, see caption), a selection of boreholes reaching or totally cutting the Pliocene series (from French borehole database, BRGM-Infoterre). Digital and simplified geology is also extracted from BRGM-Infoterre database (1:50 000 scale). The canyon rim (marine Pliocene outcrops or evidenced by boreholes) is represented by a dashed line. Notice the « island » in the « Preference » borehole area where cretaceous levels outcrops under the alluvial Rhodanian terrace. The fault source of the Le Teil earthquake (La Rouvière Fault) is indicated as a red line west of the epicentre)

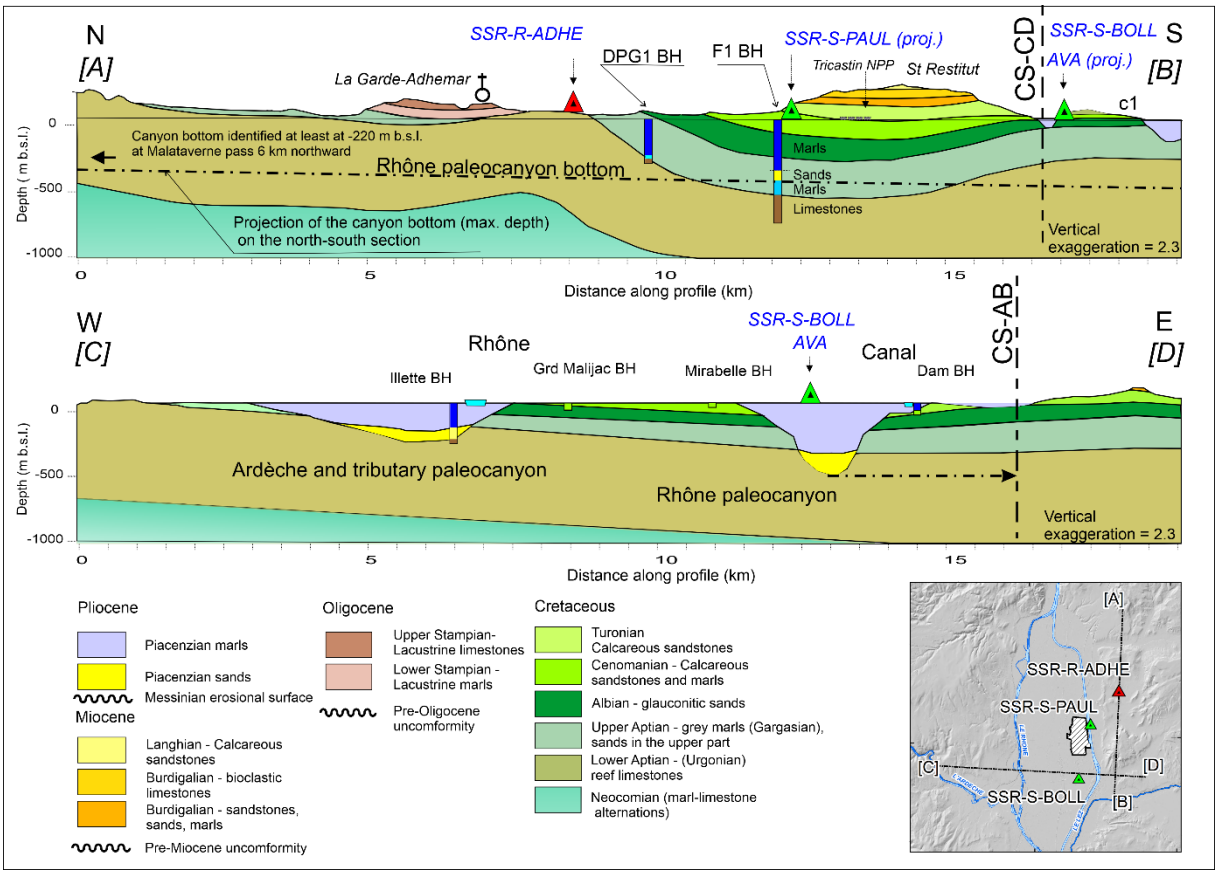

FIGURE 2: North-South [A]-[B] and East-West [C]-[D] geological cross sections located on fig 1. The low dippingdashed line is a projection of the Rhône Canyon bottom located about two kilometres west of the cross section (as indicated on the [C]-[D] cross section . The canyon bottom profile is extrapolated from borehole data (F1) and Malataverne survey done for TGV works (Mocochain et al., 2006)*. The boreholes) geology is schematically presented with the following correspondence :dark blue = Pliocene marl, yellow = Pliocene sands, light blue, green, brown = Cretaceous formations. Note that the DGP1 borehole seems to be suspended as it is probably located on the slope of the canyon. The borehole locations are indicated on fig 1.*

To complement this geological analysis, we performed NHVSR measurements using CMG-6TD Güralp velocimeters. As mentioned before, NHVSR measurements allowed us to estimate the fundamental frequency of resonance, which can be seen as a characteristic feature of the underground structure in terms of seismic response (e.g. Nakamura, 1989; SESAME team, 2004). Indeed, as found by Bonnefoy-Claudet et al. (2008), the first NHVSR peak frequency provides a good estimate of the fundamental resonance frequency whatever the peak origin (Rayleigh wave ellipticity, Airy phase of Love waves, S-wave resonance). The NHVSR curves were computed on at least 50-s-long windows spanning a 2-hour recording time using the Geopsy software (M. Wathelet, 2008; Marc Wathelet et al., 2020). The fundamental resonance frequency f0 is associated to the peak measured at low frequency on the NHVSR curves. We compute the spectral ratios by using the average of the horizontal components. Criteria of reliability based on the amplitudes and stability of the identified peaks (SESAME team, 2004) are considered to determine the resonance frequency.

At PAUL, a clear peak is identified at 0.5 Hz on the NHVSR curves (average amplitude of 4, Fig. 3, a). This peak could be explained by two major lithological interfaces identified in the F1 borehole log (Fig. 3,c): the first one at 462 m represents the interface between the sandy basal part of the Pliocene filling and the clayey marls of the Gargasian; the second interface is located at 570 m between the Gargasian marls and underlying limestones (21 m of marly limestones overlying 243 m of massive Urgonian limestones up to the borehole bottom at 834 m).

From the fundamental resonance frequency f0 given by the NHVSR measurements and the interface depth H given by the borehole interpretation, one can assess the time-average upper layer shear wave velocity Vs_{up} using the classical formula $f0=Vs_{up}/4H$ assuming a linear elastic 1D monolayer medium (Ibs-von Seht and Wohlenberg, 1999). Two simple hypotheses can be formulated depending on whether the resonance is due to one or the other of the interfaces mentioned above and considering a simple hypothesis of homogeneous Vs velocity layer. If the main interface is between Pliocene filling and Gargasian marls, the Vs_{up} velocity for Pliocene would be 924 m/s; otherwise, if the main interface is between Gargasian marls and Urgonian limestones, Vs_{up} of the whole upper series (Pliocene and Gargasian marls) would be 1140 m/s. Schlupp et al., (2001) estimated a mean Vs of 800 m/s in the Pliocene sedimentary filling in the area of Avignon, 30 km southward. Based on this, we consider that the resonance expressed by the 0.5 Hz peak observed at PAUL is due to the first interface at 462 m.

At BOLL station, the NHVSR shows a clear peak at 0.45 Hz (average amplitude of the order of 4, Fig. 3 top). This is of the same order as the fundamental resonance frequency estimated at PAUL, supporting the hypothesis that this station is located above the canyon. Based on the value of Vs inferred at the station PAUL (924 m/s), the base of the Pliocene infill beneath BOLL should be at about 510 m depth. This is deeper than the base of the canyon at PAUL, consistently with the downstream position of BOLL. Furthermore, given the depth of the top of Urgonian limestones (280-450 m, Fig. 3, c) deduced from the geological map notice information, the canyon bottom is expected to incise or at least, lies directly on top of the Urgonian limestones beneath BOLL. Therefore, we interpret the fundamental frequency at BOLL as due to the interface between the bottom of the Pliocene canyon filling and Urgonian limestones (see schematic view on Figure 3, c).

At ADHE, the NHVSR curve is almost flat and does not exceed 2 until 20 Hz (Fig. 3 top). This encounters the SESAME criteria allowing us to consider this site as a suitable “rock” reference.

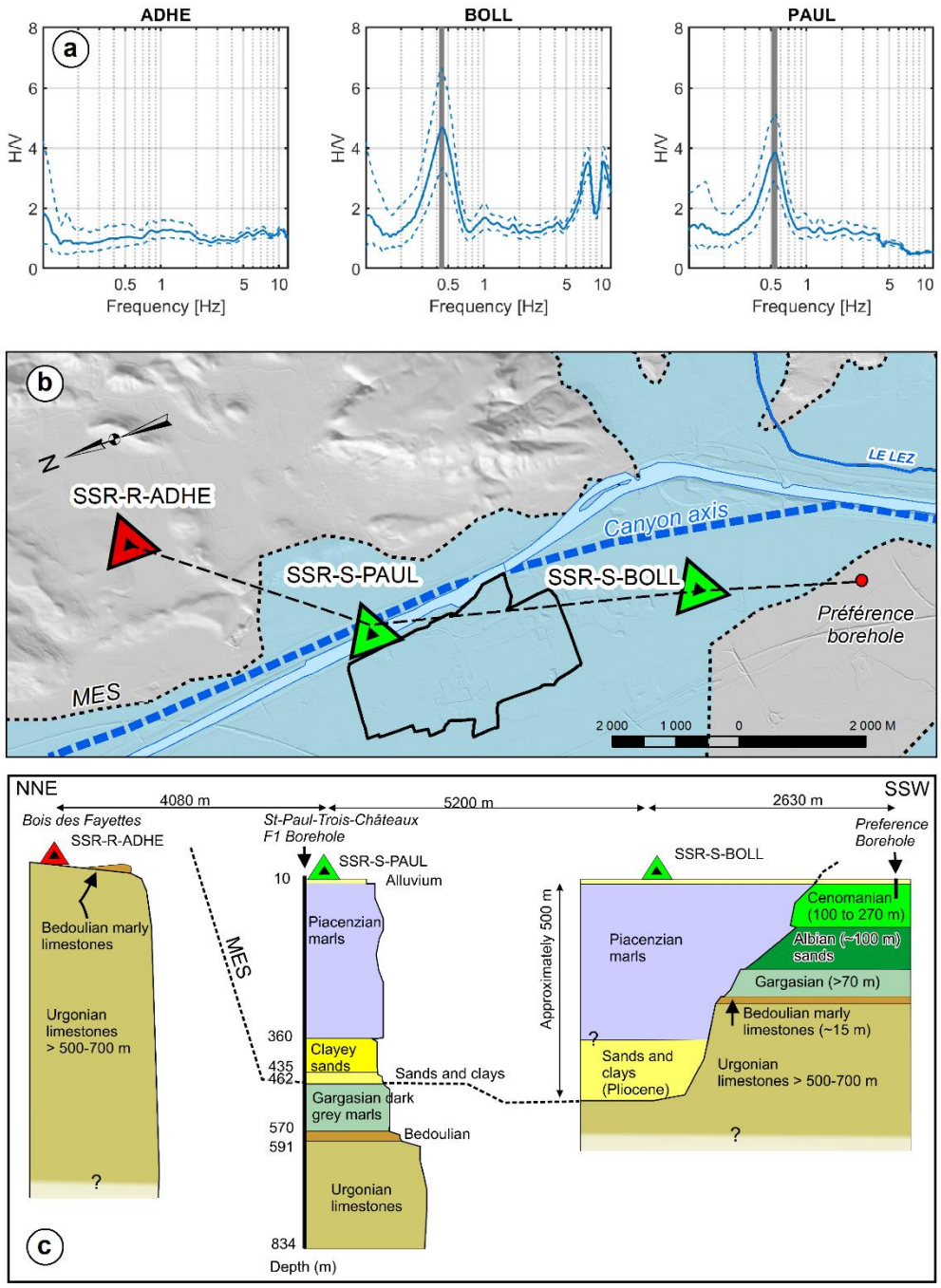

FIGURE 3: a) NHVSR curves at the 3 SSR stations from north to south that are drawn on the rotated map (b). On this map, the blue surface corresponds to the Pliocene filling limited on its edges by the black thin dotted line that corresponds to the messinien erosional surface (MES). c) Synthetic logs at the 3 SSR stations show the canyon filling and surrounding cretaceous series.

3. Empirical estimation of the seismic amplification

Perron et al., (2018) were able to assess a robust SSR in an industrial site located in Provence (Southeast France) in a low-to-moderate seismicity area. To do so, they exploited 2 ½ years of continuous recordings with the CMG-6TD broadband velocimeters as the ones used in this study. Our goals are (i) to determine whether earthquakes can also be recorded with a good signal-to-noise ratio (SNR) in the specific Tricastin industrialized area located in a zone of seismicity level fairly

equivalent to Perron et al., (2018) and (ii) to estimate ground motion amplification at BOLL and PAUL with respect to ADHE station. In addition, following Perron et al. (2018), we investigate whether ambient noise recordings could be helpful to assess this amplification.

We use continuous recordings at ADHE, BOLL and PAUL stations. ADHE recorded from 8 August 2016 to 9 June 2017, that is, 10 consecutive months. BOLL recorded from 26 October 2016 to 8 February 2017 and between 15 May and 9 June 2017. BOLL thus recorded data for 5 ½ months. PAUL station recorded from 1 September 2016 to 8 February 2017, that is, 5 consecutive months. The 3 stations were installed again from 5 November to 16 December 2019, that is, for about 1 ½ month more.

3a. Earthquake-based SSR

We use European EMSC (https://www.emsc-csem.org/) and French CEA-LDG catalogs (www-dase.cea.fr) to identify earthquakes that occurred during the recording period. If an earthquake is identified on recordings at both rock and at least one sediment station, P and S waves are picked, together with the end of the earthquake recording. We select the signal between the S wave onset and the end of the signal. We then select a noise window before the P wave, of the same duration than the selected signal. The Fourier Amplitude Spectrum (FAS) of the signal and the noise windows are then computed and smoothed using the Konno and Ohmachi filter (Konno and Ohmachi, 1998), with the usual b value of 40. We select the usable frequency band by considering a signal-to-noise (SNR) ratio threshold of 3, following Perron et al. (2017). SSR at each sediment site is then calculated in this frequency band using (Borcherdt, 1970):

$$SSR(\frac{sediment}{rock}) = \frac{FAS^{Sediment}}{FAS^{Rock}} \qquad (1)$$

where $FAS^{Sediment}$ and FAS^{Rock} are the FAS at sediment and rock sites respectively. SSR is computed for the 3 components (N-S; E-W and vertical). As proposed by Borcherdt (1970), SSR gives an estimate of site effects at the sediment station assessing that site effects at the rock site are negligible and that the source and path components of the ground motion are the same at the sediment and rock sites.

We select earthquakes providing usable frequency bands around or above the fundamental frequency f0 observed at BOLL and PAUL, that is, about 0.5 Hz. The location of these earthquakes is shown on Figure 4 (colored circles). The magnitude and distance of these earthquakes are presented on Figure 4 and Table 1. The magnitude ranges from 3.8 for local earthquakes (distance of about 110 km) to 6.4 for teleseismic earthquakes (distance of about 1200 km). These earthquakes are mainly located Southeast of the Tricastin area. Only 2 small earthquakes used to compute the SSR (2016/12/13 and 2016/12/03) are located northward. Given their magnitude and distance, these earthquakes led to small-strain ground motions in the Rhône valley. Moreover, the distance between BOLL (resp. PAUL) and ADHE being 9 km (resp. 4 km), the minimum epicentral distance is at least ten times larger than the distance between sediment and rock stations, fulfilling one main requirement of the SSR approach. SSR can thus be used to assess site amplification at PAUL and BOLL relative to ADHE.

It has to be noted that the location of the Mw 4.9 Le Teil earthquake is displayed as well on Figure 4. The very shallow earthquake (~1 km depth) led to significant damages in the area and to ground surface rupture (Cornou et al., 2020 ; Ritz et al., 2020 ; Causse et al., 2020). This earthquake was recorded at ADHE, BOLL and PAUL stations (see electronic supplement). The recorded waveforms clearly show the effect of the canyon on the seismic ground motion that is much higher and longer at BOLL and PAUL with respect to ADHE. However, because of the strength of the motion, the waveforms recorded on the CMG-6TD velocimeters were clipped. This earthquake cannot thus be used for site amplification assessment.

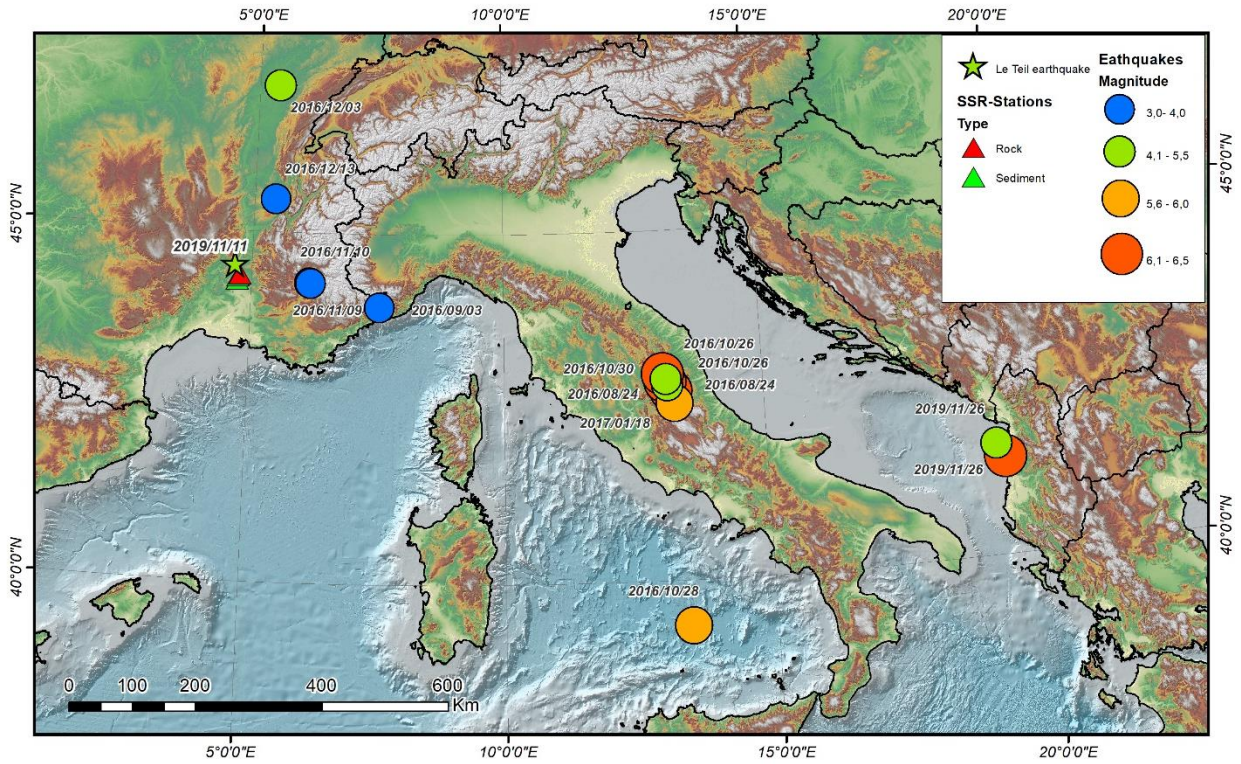

FIGURE 4: Location of the earthquakes used in this study.

Location	Date	Mag	Type	Depth (km)	Latitude (DD)	Longitude (DD)	back-azimut (N°)	Distance (km)	Source
4 km E of Norcia, Central Italy	2016-08-24	5.5	Mw	9	42.79	13.15	101	698	EMSC
3 km NE of Accumoli, Central Italy (Amatrice EQ)	2016-08-24	6.2	Mw	4	42.71	13.22	101	706	EMSC
4 km ENE of Breil-Sur-Roya, Alpes-Maritimes, France	2016-09-03	3.7	ML	4	43.96	7.55	98	226	LDG
10 km N of Norcia, Central Italy	2016-10-26	5.5	Mw	9	42.88	13.13	100	693	EMSC
3 km NW of Visso, Central Italy (Visso EQ)	2016-10-26	6.1	Mw	10	42.96	13.067	100	698	USGS
140 N of Palermo, Tyrrhenian Sea, Italy	2016-10-28	5.8	Mw	449	39.35	13.44	120	909	EMSC
5 km N of Norcia, Central Italy (Norcia EQ)	2016-10-30	6.5	Mw	10	42.84	13.11	100	693	EMSC

13 km ESE of La Motte-Du-Caire, Alpes-de-Haute-Provence, France	2016-11-09	3.8	ML	2	44.28	6.17	94	111	LDG
11 km ESE of La Motte-Du-Caire, Alpes-de-Haute-Provence, France	2016-11-10	3.9	ML	2	44.29	6.15	93	110	LDG
6 km SSE of Foucherans, Jura, France	2016-12-03	4.1	ML	2	47.09	5.41	13	306	EMSC
3 km NNW of Chabons, Isere, France	2016-12-13	3.8	ML	2	45.47	5.42	31	132	LDG
2 km, NW of Capitignano, Central Italy	2017-01-18	5.7	mb	9	42.53	13.28	102	717	EMSC
Durres, Albania	2019-11-26	6.4	Mw	10	41.38	19.47	102	1242	EMSC
30 km NW of Durres, Albania	2019-11-26	5.4	Mw	10	41.58	19.33	101	1224	EMSC

Table 1: List and characteristics of selected earthquakes used in the SSR computation

Figure 5 shows the geometrical mean of SSR values calculated for the selected earthquakes at BOLL and PAUL, plus or minus one logarithmic standard deviation. For the horizontal components, the mean SSR increases from 1 at low frequency up to about 6 at f0. At higher frequencies, the amplification globally varies between 6 and 8 at BOLL. At PAUL, it globally varies around 6 with an increase to 8 between 3 and 4 Hz for the 2 components. The N-S component also shows a decrease to 4 between 1.5 and 2.5 Hz. For the vertical component, the mean vertical SSR fluctuates between 3 and 6, with noticeable values of about 6 around 0.8-0.9 Hz and about 5 around 1.5 Hz. The associated number of earthquakes recorded in each frequency band is plotted below each SSR plot on Figure 5. It varies from a few earthquakes at the two edges of the frequency range to 9 earthquakes around 2 Hz at BOLL and 13 to 14 earthquakes at 1 Hz at PAUL.

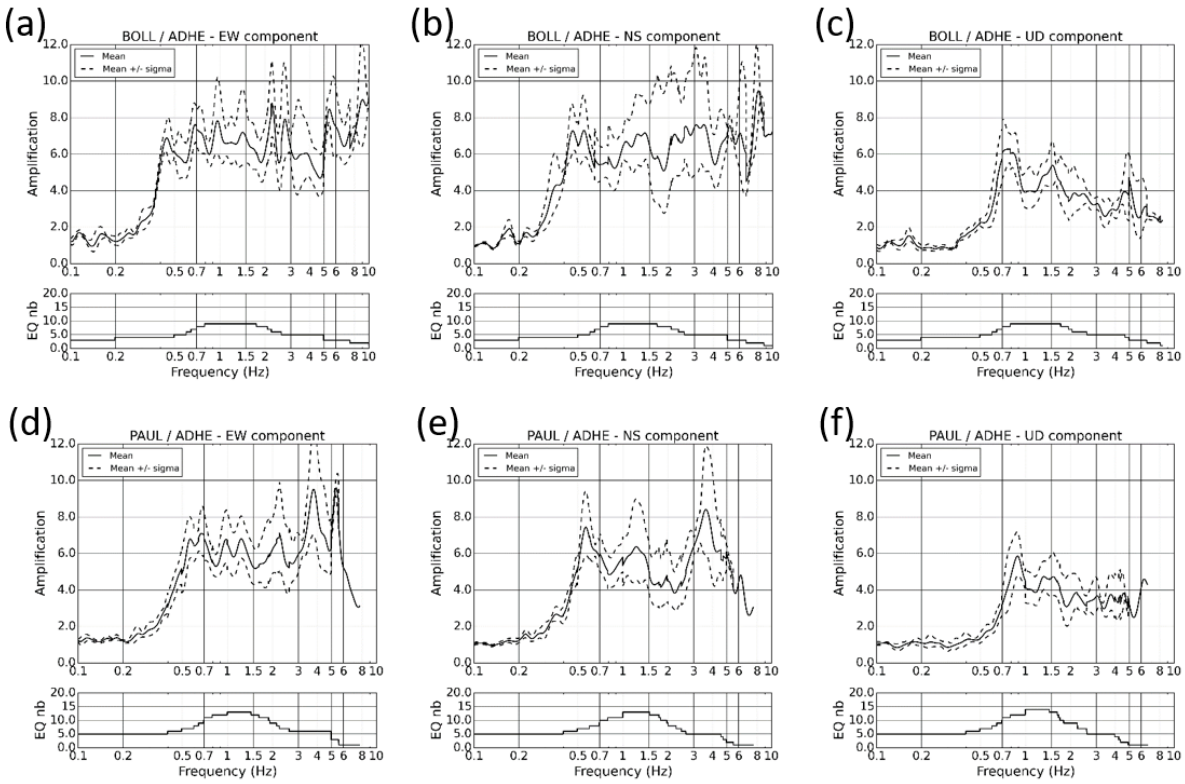

FIGURE 5: (a) Top panel : Amplification computed from Standard Spectral Ratio approach (Borcherdt, 1970) at BOLL stations with respect to ADHE station for the EW component. Mean amplification is plotted together with mean amplification plus or minus one standard deviation. The bottom panel represents the number of earthquakes used at each frequency. (b) et (c) Same as (a) respectively for the NS and vertical components. (d), (e), (f) : same as (a), (b), (c) for PAUL station.

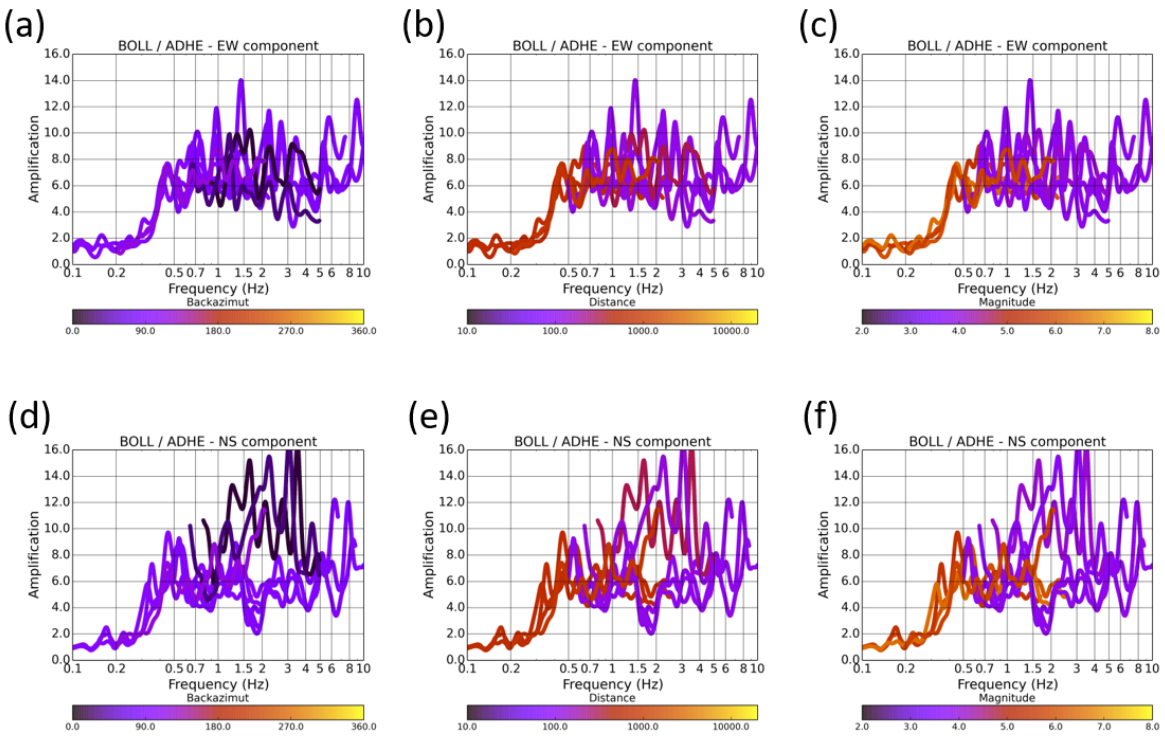

FIGURE 6 : (a) Amplification at BOLL station with respect to ADHE station computed for the EW component from individual earthquakes. The colors correspond to the backazimut of the earthquakes. (b) and (c) : same as (a) with colors corresponding respectively to distances and magnitude. (d), (e) and (f) : same as (a), (b) and (c) for the NS component.

Figure 6 shows the distribution of single-earthquake SSR as a function of the distance, magnitude and backazimuth of the earthquake, for each horizontal component at BOLL. At low frequencies, regional (~1000 km) significant (M~6) earthquakes located in the Euro-Mediterranean area (Central Italy, Albania) are predominant. At higher frequencies, local earthquakes (~100 km) of lower magnitude (M~4) located mostly within the same area (except 2 earthquakes located in Jura and Isere) are predominant. We notice a higher logarithmic standard deviation between 1 and 4 Hz on the NS component, due to SSR associated with the 2 earthquakes of different backazimuths (Jura and Isere earthquakes). This is consistent with the results by Perron (2017) that show that backazimuth and distance firstly control the SSR variability. Maufroy et al. (2016) also pointed out the influence of backazimuth and distance on the basin response. They report discrepancies between SSR computed from shallow and far earthquakes on one hand and from deep and close earthquakes on the other hand. They also notice some discrepancies between SSR computed from earthquakes located at the North of the basin on one hand and at the South on the other hand. They interpret this as being due to a different generation of surface waves at the basin edge. Such a dependency on earthquake backazimuth can be seen in Figure 6 for the NS component and could be related to the complex geological structure of the basin.

This raises the question of the minimum number of earthquakes necessary to get a robust SSR estimate in such a complex geological configuration. Perron (2017) showed that depending on the dataset, 15 to 50 events may be necessary to get a relative variation of the mean SSR less than 10% in 95% of the cases. It is likely that the limited number of earthquakes in our case does not allow to have such a robust estimate of the mean SSR in this statistical sense. SSR presented in Figure 5

should rather be seen as a first rough assessment of amplification. More data will be needed to confirm these first results and further explore the variability of SSR depending on earthquake characteristics for stations located in the canyon.

As a conclusion, these results show that regional and local earthquakes are usable to assess ground motion amplification associated with the presence of the paleo canyon in the area of Tricastin. This amplification is significant, around 6, and roughly of the same order at BOLL and PAUL stations. To our knowledge, this is the first time this amplification has been assessed. These first results provide some quantitative knowledge about the seismic response of the Tricastin area. Moreover, it confirms the possibility to get a first estimate of the ground motion amplification using earthquakes recorded for less than one year, in this highly anthropogenic and industrialized environment, despite the local low-to-moderate level of seismicity.

3b. Noise-based SSR (SSRn and SSRh)

The previous section has shown that earthquake recordings may be used to compute ground motion amplification in the Tricastin area, but still, a limited number of earthquakes are usable in this low-to-moderate seismic area. Therefore, methods based on ambient noise are of great interest for these regions. Following Perron et al. (2018), we compare SSR computed from earthquake data (we use the mean value) to SSR assessed from ambient noise data. Perron et al. (2018) tested 2 approaches: SSRn ("noise" SSR) and SSRh ("hybrid" SSR). SSRn corresponds to SSR computed using ambient noise only. Hereafter SSRn between stations PAUL and ADHE is noted SSRn (PAUL/ADHE). The SSRh approach considers a local reference station inside the basin for which an earthquake-based SSR is available. Here, SSRh is computed for PAUL station using BOLL as local reference inside the basin. SSRh at PAUL is obtained through the product of the SSRn at PAUL with respect to BOLL and of the SSR at BOLL with respect to ADHE, namely:

$$SSRh\left(\frac{PAUL}{ADHE}\right) = SSRn\left(\frac{PAUL}{BOLL}\right) SSR(\frac{BOLL}{ADHE}) \quad (2)$$

SSRn is computed using ambient noise data sliced into 1-hour files. Each 1-hour file is windowed as six windows of ten minutes. Following Denolle et al. (2013), we discard 10-min windows containing a peak that exceeds 5 times the standard deviation assessed from the 1-hour file. Overall, 1000 10-min windows are used to compute SSRn. The same processing is applied for all the SSRn estimations (i.e. also used in the SSRh computation). In the following, only mean values are presented.

Figure 7 shows SSR computed from earthquakes (similar to Figure 5), SSRn and SSRh computed at the PAUL station. First, we observe that SSR and SSRn are in good agreement up to about 0.5 Hz (i.e. f0). From 0.5 to 1 Hz, SSRn is lower than SSR at some individual frequencies for the EW and vertical components and on a larger frequency band for the NS component (amplitude of 6 instead of 7 or 4 instead of 5). SSRn remains generally between the mean SSR plus or minus one standard deviation (see Figure 5). Such similarity between SSR and SSRn is consistent with results of Perron et al. (2018) that showed that SSRn was able to retrieve f0 and A0 (i.e. the amplification at f0) for 2 sedimentary basins, in Argostoli (Greece, f0 values between 1 and 2 Hz) and in Provence (Southeast France, f0 values of a few Hertz). Here, we notice that SSR and SSRn are even in good agreement up to 1 Hz on the EW and vertical component. This limit coincides with the appearance of anthropogenic noise in ambient noise (1 Hz is usually considered as the limit). SSRn then shoots up beyond this frequency for EW and vertical components, and beyond 1.5 Hz for the NS component. Perron et al. (2018) suggest that the basin represents a natural barrier for seismic waves of frequencies greater than f0 which limits the propagation into the stiffer medium for wavefields generated within the basin, explaining

the discrepancy between SSRn and SSR for f>f0. This effect may become particularly pronounced for ambient noise at f>1Hz expected to be generated very locally. This suggests that a combination of factors (related to the geological structure as well as the generation of the ambient noise wavefield) impacts the ability of SSRn to reproduce SSR.

By contrast, SSR and SSRh show comparable amplification until 4 Hz at PAUL. SSRh is also closer to SSR than SSRn at f0 in the EW component. These results confirm the conclusions by Perron et al. (2018) that SSRh is an approach that can be used to characterized amplification up to frequencies significantly higher than the fundamental frequency. In Perron et al. (2018), SSRh was able to reproduce SSR until 10 Hz and even 20 Hz for some stations, with interstation distances varying from 1 to 2 km. Here, PAUL and BOLL stations are located at 5 km distance. This is of the same order than distances from the reference rock stations. This suggests that distance is not the key factor for the quality of SSRn. However, PAUL and BOLL are located within the same geological formation inside the canyon, which was considered by Perron et al. (2018) as a key ingredient to explain the ability of SSRh to reproduce SSR. These results are very promising and suggest that such an approach could be used within the Rhone valley on the Messinian canyon to assess amplification using either PAUL or BOLL stations as local reference inside the basin. More generally, and in the continuity of the work by Perron et al. (2018) on the two small-scale basins (width of about 1 km and depth of about 100 m), these results suggest that SSRh could also be promising in kilometer-scale basins.

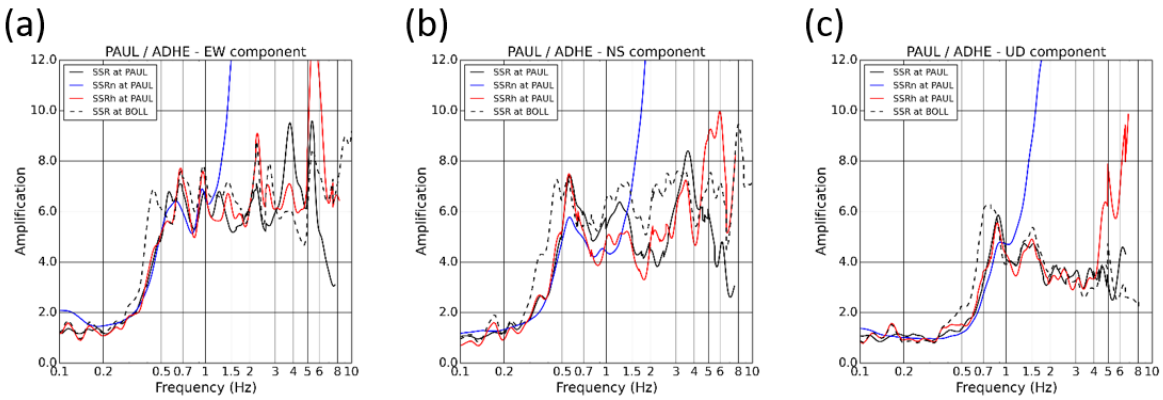

FIGURE 7: (a) Mean amplification at PAUL station with respect to ADHE station computed for the EW component from the SSR approch (black), the SSRn approach (blue) and the SSRh approach (red). SSRn computed at BOLL is added for comparison. (b) and (c) : same as (a) for the NS and vertical components.

4. Numerical estimation of the amplification based on local 1D approximation

To compare to the empirical amplification estimated in the previous section at BOLL and PAUL relative to ADHE, we compute a numerical amplification based on a local 1D approximation. This numerical computation requires 1D subsurface characterization at our station sites. We detail here data acquisition and processing for the estimation of 1D Vs profiles. The “profiles” can be as well named as “models” since they are determined from an inversion. Values considered in the numerical simulations for other geophysical parameters such as the attenuation will be presented in subsection 4c.

We used SWDA to assess 1D Vs profiles at our station sites. This approach is based on the dispersive characteristics of surface waves, meaning that different wavelengths are sensitive to different depth ranges thus giving insights into medium variation as a function of depth. SWDA is being increasingly used to determine 1D velocity profiles and Vs30, the shear wave velocity in the first 30 m (e.g., Garofalo et al., 2016; Hollender et al., 2018; Cushing et al., 2020). As mentioned in section 2, the environment of PAUL does not allow for SWDA characterization. We thus focus here on BOLL and ADHE. The acquisition configuration involved techniques and data processing may differ for the two sites for practical reasons (e.g. site accessibility and configuration) and geological configuration (very different expected Vs). The two characterization campaigns having been carried out at different times, we also took into account the feedback from the first campaign (BOLL) for the second campaign (ADHE). It is worth noting that the resulting interpretation is however very consistent from one site to the other as well as with the geological information available in the area.

4a. 1-D Vs at BOLL (sediment site)

Among SWDA techniques, the deployment of ambient vibration arrays (herein referred as to AVA) is one of the most widely used. AVA is based on the ability of seismic sensors arrays to give information about the propagation of an incident wave front (i.e. direction and velocity). It uses the easy-to-record ambient vibrations of the Earth's surface (or seismic ambient noise), which are assumed to be mainly composed of surface waves and present the advantage of not requiring artificial sources. The design of AVA acquisition configuration depends on the characterization target and medium properties. The main objectives of this campaign were to estimate 1) an average Vs of the canyon sedimentary filling, 2) the depth of the canyon bottom (expected to be about a few hundreds of meters) and 3) the Vs contrast between the sedimentary filling and the substratum.

We focused on a farming area where station arrays of several hundreds of meters can be rather easily deployed. The centre of the acquisition is still located 350 m north of BOLL because of the organization of crops and agricultural plots around the site. We used 9 Güralp CMG-6TD broadband velocimeters for the array measurements. The experimental deployment has been designed based on SESAME criteria (SESAME team, 2004) to find optimal array layout given our site configuration (accessibility, number of sensors, medium properties, depth range targeted). The chosen layout consisted of 2 arrays, whose location and geometry are shown in Figure 8a. Each array is composed of 8 CMG6-TD stations distributed on two circles (i.e. double-circle geometry with radii of 30 and 75 m for the smallest array; of 125 and 250 m for the largest) around a central seismic station. To optimize the azimuthal coverage, the inner stations are shifted by 45 degrees with respect to the azimuth of the external stations for each array. The maximal aperture of each array is 140 and 500 m, respectively. Because of the field conditions and accessibility, some adjustments have been necessary, leading to a non-perfect circle for the largest radius (Fig. 8a). The average duration of acquisition for the two arrays is 3 hours.

Data acquired have been processed using the Geopsy software package (Wathelet et al., 2020). The most stationary noise windows within the raw recordings have been selected using a STA-LTA criterion. The single sensor recordings were processed as NHVSR measurements to check the homogeneity over the array. NHVSR curves obtained do not vary significantly in shape and in frequency. This homogeneity in NHVSR measurements as well as in the local geology make us consider that the assumption of a local 1D model at the basis of the processing and inversion of AVA measurements is fulfilled. We averaged the NHVSR curves computed for each station composing the arrays and obtained an average value of f0 for the array of 0.45 Hz. One can notice that this is perfectly consistent with the value estimated at station BOLL (see section 2), supporting our assumption of using this array analysis to characterize the medium below BOLL. This value will be

used in the data inversion as characterizing the ellipticity of Rayleigh waves to constrain the depth of the main interface at the origin of the resonance.

Data were then analyzed using frequency-wavenumber (FK) techniques (e.g., Lacoss et al., 1969; Capon, 1969; Rost and Thomas, 2002). Rayleigh dispersion curves were derived from the analysis of the vertical component of ambient noise signals recorded on the arrays. Each array measurements have been analyzed and led to a dispersion curve. The analysis has been restrained within the array resolution capabilities (minimum resolvable wavenumber at low frequencies and aliasing limit at high frequency) that are controlled by the array geometry (M. Wathelet, 2008). For the 2 arrays, the dispersion diagrams show a single dominant mode that we interpret as the fundamental Rayleigh mode. The dispersion curves extracted from each array measurements are very consistent within the common frequency ranges (1.5-2.5 Hz), strengthening our assumption that the individual curves reflect the same propagation mode. These two curves are thus combined to provide a broader frequency-band dispersion curve (0.5-5 Hz). Figure 8b shows this average curve as well as the associated uncertainties observed at each frequency.

We used the dinver software, part of the Geopsy package (Wathelet et al., 2020) to invert the dispersion curve and estimate a 1D Vs profile below BOLL. This software uses a global search approach with a neighborhood algorithm (Wathelet, 2008). In order to add some information on the interface depth between the sedimentary filling and the substratum, the resonance frequency estimated from NHVSR computed over the array stations (f0=0.45 Hz) is taken into account, and jointly inverted as Rayleigh-wave ellipticity peak with the array-based dispersion curve. An uncertainty of 0.05 Hz was associated with f0. We considered equal weight for the dispersion curve and the resonance frequency in the inversion process. We estimated the thickness of the first layer and the maximum resolution depth using usual rules of thumb, that is, considering one third of the minimum and maximum observed wavelengths, respectively. This results in a model resolvable depth ranging from 35 m down to about 540 m. Different parameterizations were tested, especially regarding the number of layers used. We found that 4 layers were necessary to reproduce the observed dispersion curves, especially at low frequency, which constrains the velocity at depth (i.e. in the basement). Surface waves are mainly sensitive to Vs and layer thickness. Regarding other parameters, we assumed a fixed density of 2.2 and a Poisson ratio varying between 0.2 and 0.5 for the inversion.

Figure 8d shows the 8610 velocity models whose misfit is inferior to 1. The misfit represents the RMS (Root Mean Square) difference between the forward-modelled parameters and the measured ones normalized by one standard deviation. The parameters are the dispersion curve of the fundamental model of Rayleigh waves and the Rayleigh wave ellipticity peak considered as a good indicator of the fundamental resonance frequency. This comparison is also illustrated in Figs 8b and c showing a good agreement. The resulting models are characterized by a surface layer (fixed at 35 m) with a mean Vs of about 500 m/s with a standard deviation of 65 m/s. It is worth noting that these values could give a first order estimate of Vs30 and associated uncertainties in this model that cannot resolve exactly the upper 30 m. This first 35-m deep layer overlies a layer of approximately 70 m with Vs ranging from 680 to 850 m/s. We then have 2 layers with Vs slightly increasing from 950 m/s to about 1050 m/s reaching the depth of 500 m. We there found an interface corresponding to the sediment/bedrock interface whose depth is situated between 490 m and 590 m, with an average value of 534 m and a standard deviation of 47 m. The mean velocity in the sediment layer is 844 m/s and the associated standard deviation is 46 m/s. The underlying velocity is found difficult to determine precisely in view of the theoretical maximal solvable depth of about 540 m. The velocity

models shown in Figure 8d suggest however a strong velocity contrast at this interface with underlying velocities characterized by a mean Vs of 3132 m/s with a standard deviation of 287 m/s.

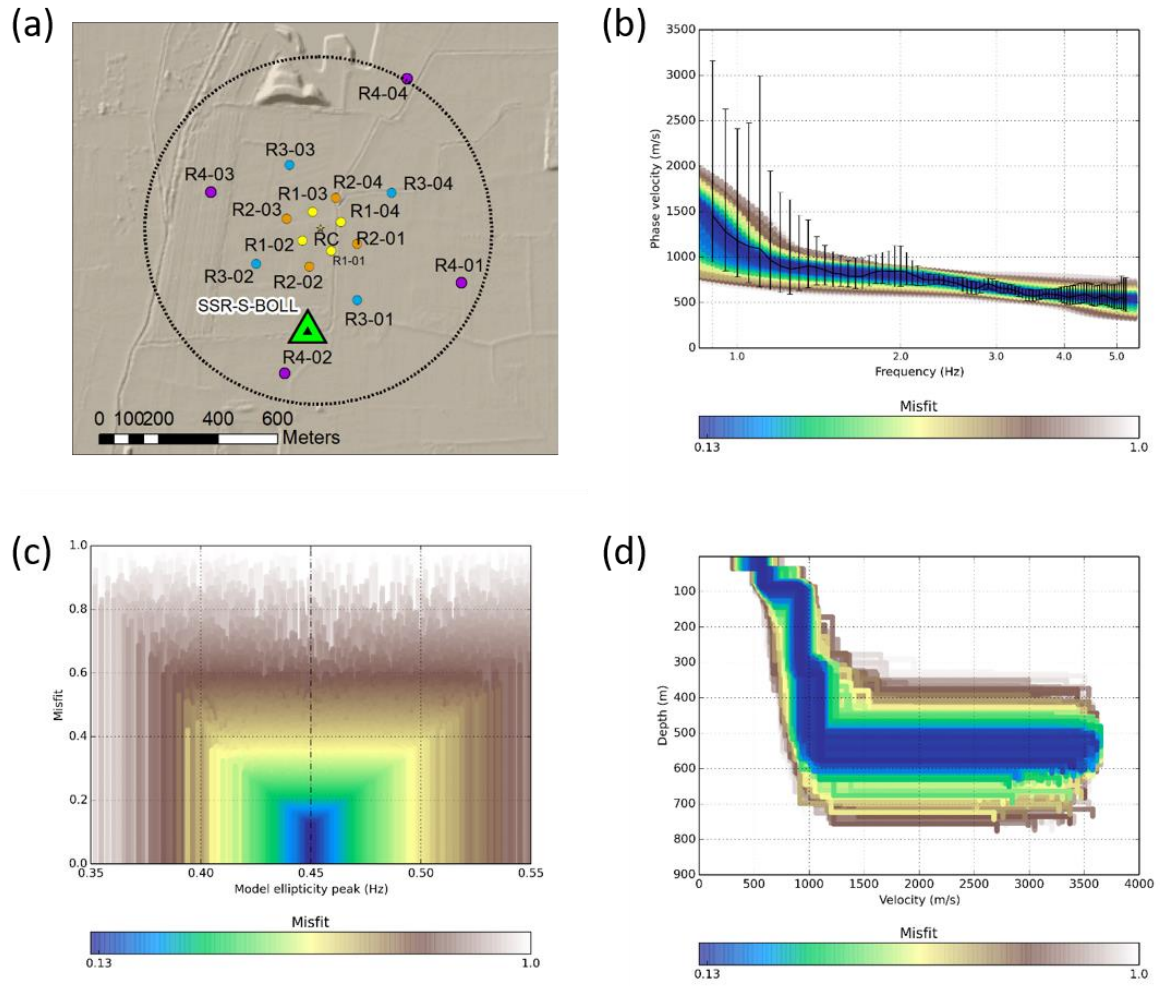

FIGURE 8: Site characterization at BOLL. (a) Geometry of the ambient vibration arrays (AVA) involving 2 double-circle arrays (R1-R2 and R3-R4) around a central station RC. Because of site constraints, RC is located 350 m north of BOLL (green triangle). (b) and (c) Comparison between the observations and forward modelling associated with velocity models estimated from the inversion and shown in (d): (b) The black curve shows the observed dispersion curve of the Rayleigh fundamental mode and its uncertainties. The coloured curves correspond to the forward-modelled dispersion curves. Colour stands for the misfit value in (b), (c) and (d). (c) The black line points to the measured fundamental resonance frequency f0 estimated at BOLL using NHVSR (section 2). Coloured lines indicate the forward modelled peak of Rayleigh ellipticity (see text for discussion). (d) 1D Vs models obtained from the inversion process.

4b. 1-D Vs profile at ADHE (rock site)

ADHE station being surrounded by dense vegetation, it was not possible to carry out SWDA measurements at the exact station location neither. We had to shift about 400 m apart from the exact station location. However, the geological configuration of the limestone slab under the SSR

ADHE station, the MASW site location and the AVA (see below) is very similar (all measurement locations are located on the same structural surface of the Urgonian limestone).

As for BOLL, we used AVA to estimate the 1D Vs profile at depth. ADHE being located on the Urgonian limestones whose Vs is expected to be very high (~2000 m/s), this will naturally pull the AVA-based characterization towards larger depths for a given array geometry in comparison with sediment sites (like BOLL). To complement the AVA approach and thus our characterization at shallower depths in this specific context, we use the Multichannel Analysis of Surface Wave approach (MASW, Stokoe et al., 1994; Park et al., 1999; Hollender et al., 2018) in which geophones are placed along a line and surface waves were generated by hitting the ground with a sledge hammer. Using these complementary methods should also allow us to obtain an estimate of Vs30 at ADHE.

AVA

We used 11 Güralp CMG-6TD broadband velocimeters for AVA measurements in this second campaign. Once again, the experimental deployment has been designed based on SESAME criteria. The chosen layout consisted of 3 arrays: 1 circle involving 10 sensors and a central station (radius of 210 m); and 2 double-circle geometry with increasing paired radii (60 m and 120 m; 120 m and 210 m) involving 2x5 sensors equally spaced around 2 circles and the central station. Figure 9a shows the measurement points belonging to R3, R2 and R1 whose radius are respectively 210 m, 120 m and 60 m. As for BOLL, the azimuth of the sensors for the larger circle was shifted with respect to the azimuth of the sensors for the smaller circle, to optimize the azimuthal coverage of the whole array. The layout is shown on Figure 9a. The central station is located 480 m away from ADHE. For each array, the acquisition lasted for a few hours (the larger aperture arrays, the longer the acquisition duration).

Data acquired has been processed using the Geopsy software package (Wathelet et al., 2020) and the same pre-processing as for BOLL, namely using a STA-LTA criterion for selecting stationary windows and computing NHVSR on each array station. The amplitude of NHVSR curves remains smaller than 2 for most of the stations, satisfying the SESAME criteria for rock sites (SESAME team, 2004). Moreover, the topographical maximal slope is less than 5% in the measurement area and geological structure is relatively flat (dip ~5° N). This homogeneity in NHVSR measurements as well as in the geology configuration make us consider that the assumption of a local 1D model is fulfilled. Similarly, to the processing at BOLL, AVA measurements were then analyzed using frequency-wavenumber (FK) techniques and the Geopsy software. Rayleigh dispersion curves were derived from the analysis of the vertical component of continuous data. As for BOLL, the curves obtained from the different array measurements showed a good agreement within their shared frequency range. This allowed us to build a unique curve between 4 and 25 Hz we interpret as the dispersion of the fundamental mode of Rayleigh waves.

MASW

The MASW acquisition was set up southeast of the AVA arrays, along a nearby dirt road. This is placed at around 400 m distance from the ADHE station on the same geological unit following the geological map. 24 4.5 Hz 1C vertical geophones were positioned along the road with a 2-meter interval. The distance between the closest receiver and the shot position was fixed successively to 2 meters and then 10 meters at both ends of the seismic line. In Figure 9a, points named Masw-0m and Masw-66m correspond to the two extreme shot positions and Masw-33m is located in the middle of these two extreme positions. For each shot position, the shots generated by a sledgehammer were repeated 10 times to increase the signal to noise ratio. We computed Rayleigh

waves dispersion diagrams from MASW data following Bitri et al. (1998), Gelis et al. (2005) and Park et al. (1999). We were able to pick manually the dispersion curve of the fundamental mode of Rayleigh waves between 105 and 183 Hz. These frequencies lie between the aliasing limit evaluated according to the criterion of Foti et al. (2018) and the maximum resolvable wavelength due to the length of the seismic line evaluated according to the criterion proposed by Bodet (2005).

One can notice that the dispersion curves derived from our 2 approaches (AVA and MASW) cannot provide any velocity information between about 25 and 100 Hz (Fig. 9b). This gap in the dispersion curve implies that the model obtained from the inversion of this composite dispersion curves will present a large uncertainty on a portion of the depth range investigated. This will be kept in mind while interpreting the resulting models.

Inversion

We again used the dinver software of the Geopsy package (Wathelet et al., 2020) to invert the obtained dispersion curve. We tested different parametrizations for the velocity models. This time, we needed a 10-layer model to reproduce the observed dispersion curves, especially at low frequencies. Density was fixed at 2.5 and the Poisson ratio may vary between 0.2 and 0.5. Figure 9c shows the 1148 velocity models obtained whose misfit is below 1. Using the rule of thumb of one third of the minimum and maximum wavelength to estimate the resolvable depth range, the dispersion curves suggest that AVA (resp. MASW) measurements will constrain the Vs model between the depth of about 30 m and 230 m (resp. within the first 5 meters). This suggests a poor resolution of the model for depth ranging from 5 to 30 m. This shows that contrary to what we expected, AVA measurements were able to provide an average information within the upper 30m (and hence Vs30). This comes from the possibility in this case to process ambient noise data up to 25 Hz which is rather high and may not anticipated since it completely depends on the nature of the ambient noise at the site of interest.

Once again, the dispersion curves computed from the resulting models fit well our observations, both at low and high frequencies and support the robustness of these results (Fig. 9b). In these models, Vs regularly increases with depth, from about 1000 to 1500 m/s at the surface to 2700 to 3600 m/s at 200 m depth. The mean velocity at depth is equal to 3180 with a standard deviation of 252 m/s. Such high velocity values at depth are consistent with the presence of Urgonian limestones whose thickness is estimated in this area as ~700 m from geological investigations. Relatively lower velocity values close to the surface are interpreted as the effect of surficial weathering effects due to erosion on Urgonian limestones. Figure 9d shows the Vs profiles in the first 30 meters. The mean Vs30 value extracted from these models is equal to 2016 m/s with a standard deviation of 122 m/s. This high Vs30 value is an indicator of a hard rock site, which is consistent with the hardness of Urgonian limestones observed on field. It is also consistent with other Vs30 measurements on hard limestones found in Southeast France: Vs30 of 2100 m/s in Cretaceous limestones (Perron et al., 2018) and of 2090 m/s in the Upper Jurassic (Tithonian) limestones (Hollender et al., 2018). This follows most criteria of Felicetta et al. (2017) and is a further support to use this site as a reference rock site.

It is worth noting that the velocity profile at depth estimated at BOLL can be discussed in the light of these results. Indeed, the Vs estimated in the substratum below BOLL tends to show similar values (even if it is associated with large uncertainties). This is totally consistent with Vs estimated for Urgonian limestones at ADHE and with the geological interpretation detailed in section 2 suggesting that Pliocene directly overlies Urgonian limestones at the bottom of the canyon, below BOLL. This somehow strengthens the presence of Vs as high as 3000 m/s within the substratum below BOLL.

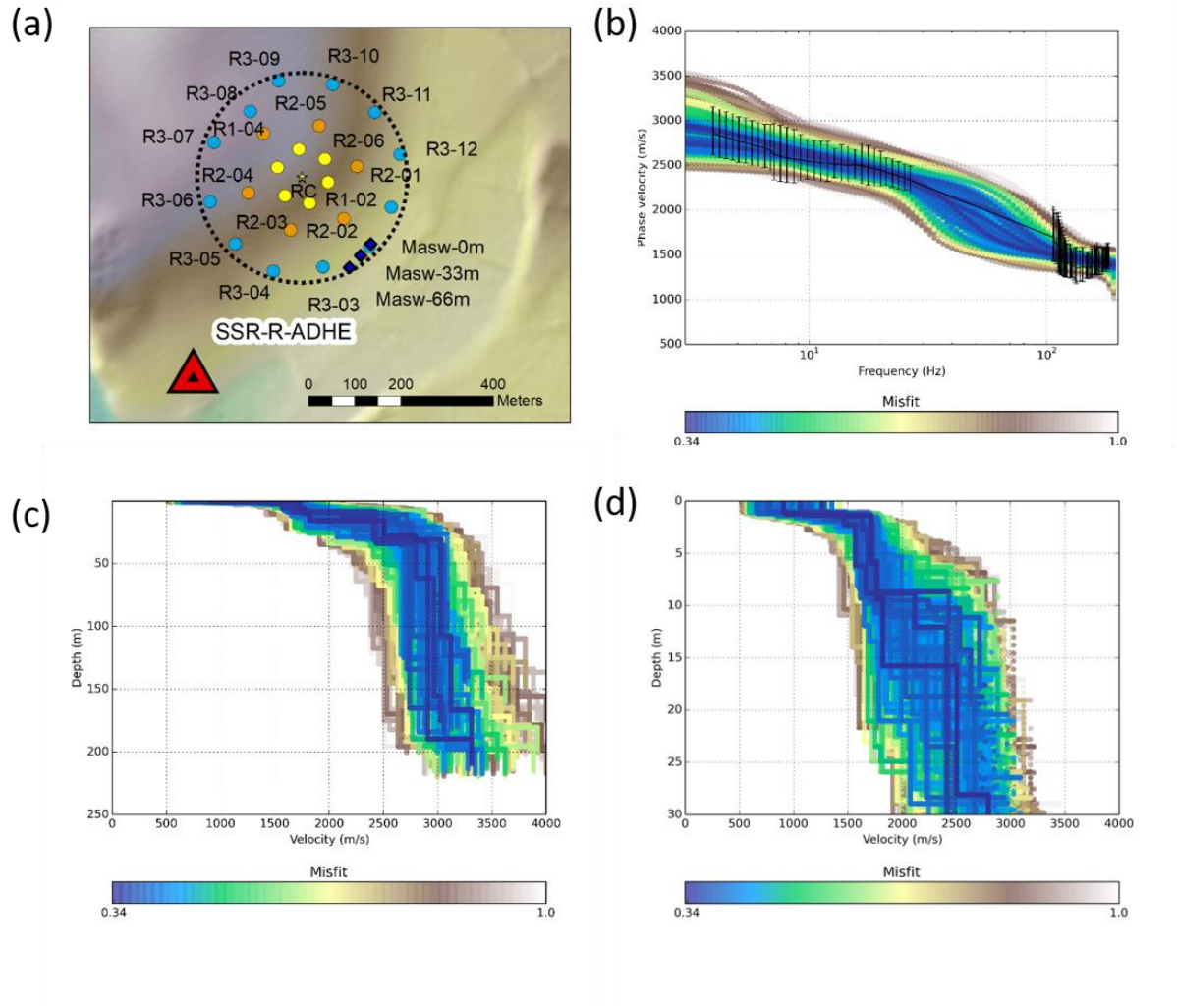

FIGURE 9: Similar to Figure 7 for ADHE. (a) Geometry of the ambient vibration arrays (AVA) involving 3 arrays: 1 circle (R3) and 2 double circles (R2-R3odd and R1-R2) around a central station RC. Because of site constraints RC is located 480 northeast of ADHE. R3odd corresponds to the 5 sensors of odd index in R3. The location of MASW measurements is shown in dark blue. (b) The black curve shows the measured dispersion curve of the Rayleigh fundamental mode and its uncertainties, resulting from the processing of AVA and MASW measurements. The coloured curves correspond to the forward-modelled dispersion curves associated with 1D Vs models estimated from the inversion (c). (c) and (d) respectively show the Vs models until the maximum inverted depth and in the first 30 meters. Colour stands for the misfit value in (b) and (c).

4c. Numerical amplification based on the derived 1D profiles

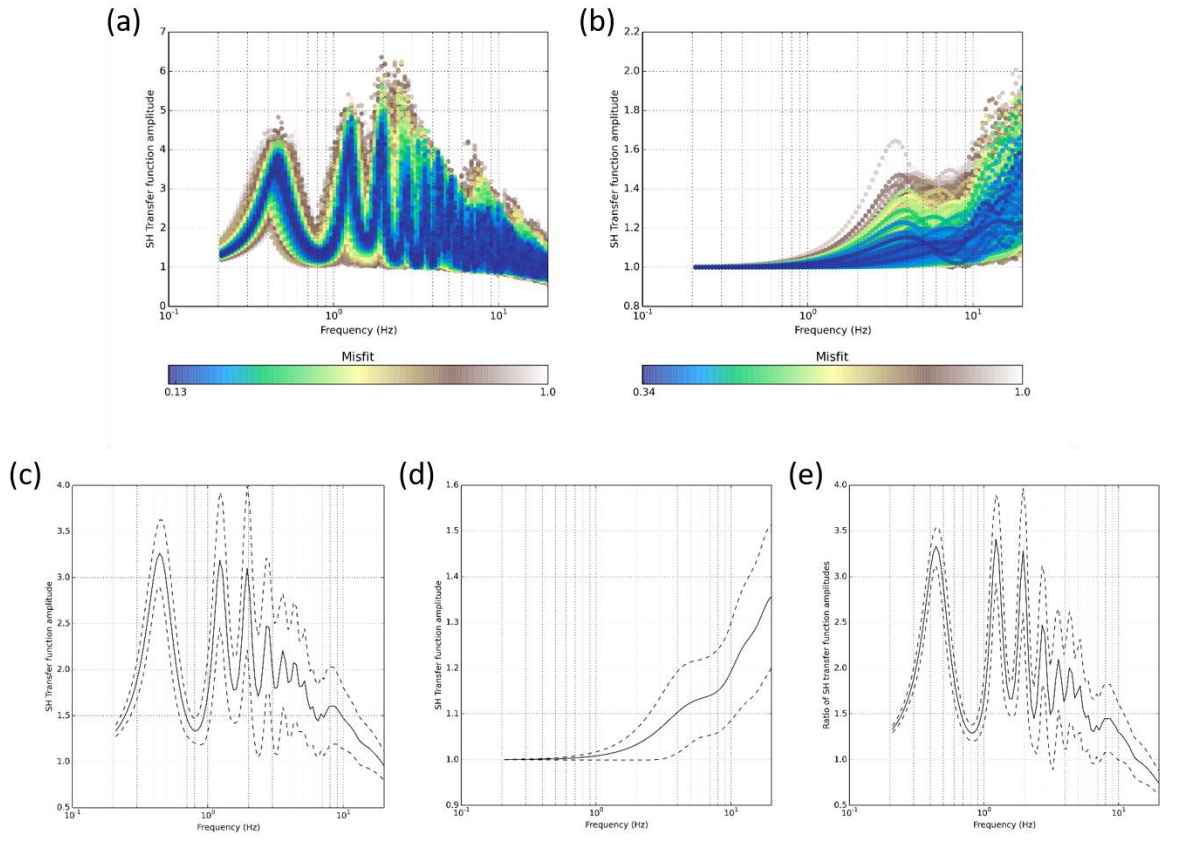

FIGURE 10 : (a) and (b) Transfer functions computed from 1D models presented respectively in Figure 8 for BOLL and Figure 9 for ADHE. (c) and (d) mean transfer function and mean transfer function plus or minus one standard deviation for 1D models with misfit lower than 1 respectively at BOLL and ADHE. (e) Mean ratio of transfer functions plotted in (c) and (d) and mean ratio plus or minus one standard deviation.

In this section, we are interested in assessing ground motion amplification and its variability from the 1D velocity profiles obtained in sections 4a and 4b. Teague and Cox (2016) investigate three approaches to take into account the variability and accuracy of Vs estimates for site response analysis. They (i) use Vs profiles obtained from dispersion curves inversion, (ii) modify the true model considered as the best-case Vs profile by 20% to obtain upper/lower range profiles and (iii) randomize this best-case Vs profile using the approach of Toro (1995). Using these three approaches to account for Vs variability, they found that the first approach gives a lower variability than the last one in terms of dispersion curves and transfer function. The dispersion curve is better fitted in the first case than in the last case while dispersion curves are shifted in the second case. They conclude that, as long as the observed dispersion curve is well-fitted and that different parametrization have been tested, Vs profiles obtained from surface wave inversion provide a means to account for Vs uncertainty. In our study, velocity profiles computed from surface wave inversion at BOLL and ADHE (Fig. 8 and 9) fit well the dispersion curves and different model parametrizations have been tested. Therefore, we follow the first approach proposed by Teague and Cox (2016) to account for Vs variability and include this variability in site response analysis. In the following, we compute the site response for each model presented in Figure 8 for BOLL and 9 for ADHE. The inter-model variability is quantified through the standard deviation of transfer functions.

For each 1D model we compute the transfer function corresponding to the ratio of the Fourier Amplitude Spectra at the surface and at depth. To that purpose, the wave propagation for vertically

incident waves is computed using the code « gpsh » from the geopsy software (Wathelet et al., 2020), that can directly use the models resulting from the inversion process as input. This code is based on the reflectivity method (Kennett and Kerry, 1979) as implemented in P.-Y. Bard and Gariel (1986) and Theodulidis et al. (1996). As a simple comparison, we computed also the transfer function using the Haskell-Thomson method (Haskell, 1950, Thompson, 1953) that shows a good agreement with the one obtained with gpsh. We introduce attenuation in the models through the quality factor Qs for S waves. We consider Qs equal to 50 at BOLL and 100 and ADHE as first order approximation. It is worth noting that using these values, or Qs equal to one tenth of Vs that could alternatively be used as first rough approximation, does not change conclusions presented hereafter.

Figure 10 shows the transfer functions obtained using the set of 1D velocity profiles estimated at BOLL (Fig. 8) and ADHE (Fig. 9). At BOLL, the transfer functions present several distinct peaks (Fig. 10a). The first amplified frequency, corresponding to the fundamental resonance frequency, is estimated at around 0.45 Hz, consistently with the value used in the inversion process. The mean amplitude is 3.2 and ranges from 3 to 3.5 when the inter-model variability is taken into account (Fig. 10c). We observe a second and third peaks respectively at 1.2 Hz and 1.9 Hz. The mean amplitude of these peaks is about 3 and ranges from 2 to 4 (Fig. 10c). The amplitude variability is therefore larger than for the first peak. At higher frequency, the inter-model transfer function variability increases. This is consistent with results by Foti et al. (2009) that study transfer functions computed using 1D velocity profiles coming from the inversion of a single dispersion curve: they found that the resulting transfer functions are similar at low frequency and that the variability increases with frequency due to the inter-model variability. The inner structure of the sedimentary filling could have an influence on the 1D transfer function at high frequency. Our experimental configuration and inversion process prevent us from getting high-resolution knowledge of the sedimentary filling. We thus focus our interpretation on the low frequency part of the transfer function, especially its amplitude and shape around the first amplified frequency. In other words, in the assumption of a local 1D geometry, we consider that the mean Vs and thickness of the sediment layer together with the Vs contrast with underlying bedrock are trustful. On the other hand, the impact of the inner structure of the sedimentary layer at BOLL is considered as secondary in our analysis.

At ADHE, both the transfer function amplitude and its variability increase with frequency (Fig. 10b). However, the mean transfer function plus one standard deviation is lower than 1.5 on the whole frequency band (Fig. 10c); it is about 1 at 0.45 Hz.

In an attempt to assess the ground motion amplification at BOLL taking ADHE as a reference, we select pairs of (sediment, rock) velocity profiles that show similar velocities at depth (i.e. with a difference lower than 10 m/s), implying a similar modelled ground motion. To reduce computation costs, only velocity models with a misfit lower than 0.5 are considered. Then, for each of the selected velocity pairs, we extend the velocity profile at the rock site, so that the velocity profile at ADHE is as deep as the one at BOLL. The amplitudes of the corresponding transfer functions are slightly lower for ADHE site (mean value is 1.3 in Figure 10b instead of 1.35 at 20 Hz in Figure 10d) since the calculated ground motion is more attenuated at the surface due to a larger propagation distance. Finally, we compute the ratio between the transfer functions obtained at BOLL and ADHE (Fig. 10e). This ratio is an approximation of the amplification between BOLL and ADHE. At the first order, it is similar to the transfer function at BOLL because of the low amplitude of the transfer function at ADHE. In particular, mean amplification at 0.45 Hz is about 3.3, and inter-model amplification ranges from 3 to 3.5.

To conclude, we use the 1D velocity profiles at BOLL and ADHE to assess the ground motion amplification between these two stations around the first amplified frequency. In the next section,

we discuss how this numerical amplification, based on the assumption of a 1D local geometry, compares to the empirical one estimated from earthquakes recordings in section 3a.

5. Discussion on the comparison between the empirical and numerical amplifications at low frequency

In this section, we focus our comparison on the amplitude and shape of the transfer function around the first amplified frequency in order not to overinterpret the higher frequency part of the numerical curve which is tainted with more uncertainties as discussed above. The first amplified frequency f0 is 0.45 Hz for both estimations but the mean value is different: about 6 for the empirical estimation (section 3a) and about 3.3 for the numerical one (section 4c). Moreover, the amplification computed using 1D velocity profiles presents a peak around 0.45 Hz whereas the empirical amplification shows a plateau-like shape. It is worth noting that, this observation remains true even at higher frequencies. Decreasing the smoothing used to compute empirical amplification leads to more pronounced peaks at some frequencies. However, it does not improve the comparison between empirical and numerical amplifications neither in shape nor in amplitude.

The observed discrepancies between the empirical and the numerical amplifications at low frequencies could have different explanations:

1. Inacurracy in 1D velocity models. The model parametrization is kept simple in our inversion process and the resulting resolution is limited. However, our analysis allows us to consider the mean velocity in the sedimentary filling well constrained by the inversion process and the velocity at depth trustful (in particular given the consistency with ADHE, see discussion in section 4b). Reaching an amplification of 6 at the fundamental frequency with 1D velocity models would require to either decrease the mean velocity in the basin or increase the velocity in the bedrock. While the latter seems unlikely given the very high velocities, the former would imply a reduction of velocity by a factor of 1.5-2 (amplification ratio between empirical and numerical assessments) that will not allow to fit the observed dispersion curve. Moreover, a decrease in velocities would also lead to a shallower interface between sediments and bedrock to preserve the fit with the ellipticity peak. As explained in section 2, a geological interface at about 535 m depth is consistent with information from deep boreholes and geological data. Therefore, an interface shallower by a factor of 1.5-2 seems to be unlikely as well.

2. Incidence angle of the incoming wavefield. The incoming wavefield may be not vertical as used in numerical simulations but inclined. A vertical incident angle is compatible with regional and teleseismic events. As a sensitivity study, we change the angle of incidence from 0 (vertical incidence) to 20 degrees using the Haskell-Thomson (Thompson, 1950; Haskell, 1953) method. The amplitude and shape of the obtained transfer function are very similar to the ones shown in Figure 10a. Perron (2017) found an influence of the earthquake epicentral distance on amplification in the Argostoli basin. But these differences are observed for distances lower than 26 km, that is much shorter than the minimal distance of about 110 km considered in our case. The discrepancies observed between amplifications computed with different earthquakes in section 3a seems to be rather related to the influence of the earthquake azimuth (Fig. 6).

3. small-scale variations of subsurface properties (e.g., velocities): these heterogeneities are not taken into account in our 1D simulations. They could however lead to wave scattering and transfer

functions modification. Such phenomenon could be taken into account using frequency-dependent attenuation. Alternatively, small-scale heterogeneities can be introduced in models. Among others, Thompson et al. (2009), El Haber et al. (2019), Tchawe et al., (2021) have shown that the impact of these heterogeneities depends on their properties. In particular, El Haber et al. (2019) compute the wave propagation in a model composed of a sedimentary layer above a homogeneous bedrock. The sedimentary layer is defined by strong perturbations of velocities (coefficient of variation of 40%). Hundred random realizations of this medium are generated in which the wave propagation is computed. The mean first amplified frequency and corresponding amplification are modified by around 25% and 30% respectively with respect to the homogeneous model. At high frequency, these perturbations lead to a mean transfer function that corresponds to a smooth version of individual transfer function among frequencies. Moreover, Thompson et al. (2009) observe a reduction of amplification at the first amplified frequency when accounting for small scale heterogeneities with a coefficient of variation of 25%. Given that the discrepancy between modelled and observed amplification at BOLL is at least 50%, we consider that material heterogeneities could explain part of the discrepancy between numerical and empirical amplifications at BOLL, but it is reasonable to think that other processes also play a role. A precise quantification of these effects would require more data (e.g., velocity measurements in boreholes, CPT/SPT dense measurements in the area, ambient noise dense acquisitions).

4. The 2D/3D geometry of the basin. The complex geometry of the basin could explain discrepancies between observed and modelled ground motion because other waves than shear waves with a vertical incidence propagate inside the basin. Indeed, the shear wave velocity reduction leads to ground motion amplification (lithological effects). Other phenomena, such as 2D/3D resonances, or propagation of waves generated at the basin edges, could also occur (Kawase, 1996; Cornou and Bard, 2003; Roten et al., 2006; Michel et al., 2014). In order to get an idea of the main propagation regime in the vicinity of BOLL, we use the approach of Bard and Bouchon (1985). Assuming that the basin is the deepest at BOLL in the area, the basin depth (h) ranges from 486 to 581 m (mean depth plus or minus one standard deviation from the 1D velocity profiles) and the basin width (w) is about 4 km according to geological data. The basin shape ratio ($2 \times h/w$) therefore varies between 0.24 and 0.29 in this area. The velocity contrast at depth varies between 3.38 and 4.05. Following the Bard and Bouchon (1985) criterion, Figure 11 suggests that 1D resonance combined with lateral propagation is the dominant regime. This is a first approximation since the basin geometry may be strongly different from the sinus-like shape used in Bard and Bouchon (1985), with sharp basin edges for example.

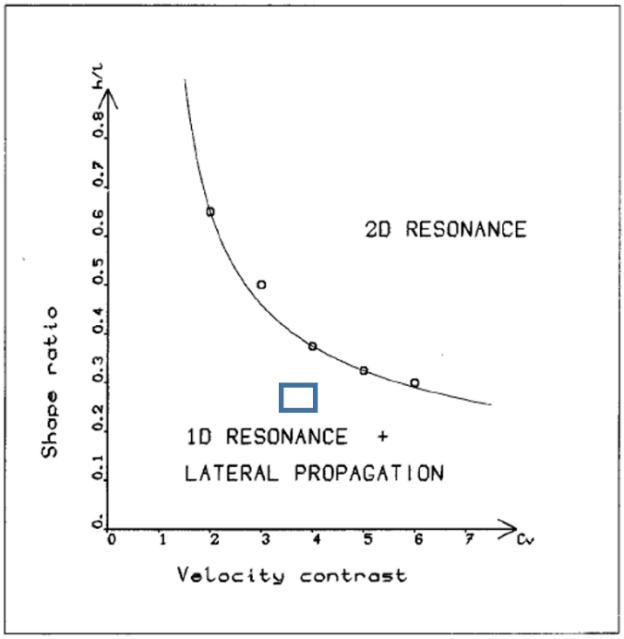

FIGURE 11: Shape ratio as a function of velocity contrast delimiting two kinds of resonance in basins as defined by Bard and Bouchon (1985). Parameters estimated at BOLL stations correspond to the blue rectangle.

Several studies have examined the influence of such edge-generated waves on the amplification. In the Gubbio basin in Italy, Bindi et al. (2009) propose that the amplification at f0 could be due to 1D resonance effects together with edge-generated surface waves that propagate within the basin. This interpretation is based on Earthquake Horizontal to Vertical Spectral Ratio (EHVSR) whose peak occurs at f0 with an amplitude of about 6 whereas SSR amplitude is about 10. Similarly, EHVSR amplitude at f0 estimated at BOLL and PAUL is about 4 and lower than SSR amplitude of about 6. In the Grenoble basin in France, Cornou and Bard, (2003) attribute energy discrepancy between numerical amplification in a 1D model assessed from borehole measurements and empirical amplification computed from earthquake recordings to the presence of diffracted waves from the basin edges above f0. The reference station is located at depth in a borehole but this conclusion could also hold for reference stations located at the surface. Mascandola et al. (2021) compare transfer functions computed from 1D velocity profiles to empirical ones obtained from earthquake recordings at surface and depth at 4 locations inside the Po Plain in Italy. For one of these stations, they observe an underestimation of the numerical transfer function with respect to the empirical one of up to 60% at low frequency. They correct for the basin effect using a correction term that accounts for the generation of surface waves at the basin edges in the GMPE of Lanzano et al (2016) calibrated for the Po Plain area and Northeastern Italy. Such correction allows them to better fit the empirical transfer function. At last, Michel et al. (2014) compute the transfer functions from 1D velocity profiles determined from array measurements. They compare them with the amplification deduced from the difference between predicted ground motions at a generic rock and observed ground motions, representative of the site response. This comparison is made in terms of the presence of peaks (smooth vs peaky curves), corresponding frequency values, and the level of amplification over the whole frequency band. It is then used to determine whether the site has a 1D response and if edge-generated waves propagate. Even if we focus our analysis and discussion on the low frequency part (amplification and shape around the first amplified frequency), we note that, following Michel et al. 2014's approach, the plateau-like shape of the empirical amplification together with its larger amplitude value over a large frequency band favor the interpretation of differences between

empirical and numerical amplification as due to the presence of edge-generated surface waves propagating inside the basin.

To summarize, the available information tends to suggest that edge-generated waves may have a strong influence on the local basin response at BOLL and PAUL. However, the available local 1D characterization is not sufficient to quantify their actual impact. Imaging the whole canyon geometry and determining its properties appears to be necessary and is foreseen as a follow-up of this study. It would allow to perform 3D numerical simulations of wave propagation inside the area to better understand the influence of edge-generated waves and its impact on the empirical amplification within the basin. The role of wave scattering due to small scale heterogeneities could also be addressed in a further step.

Conclusions and perspectives

In this paper, we presented seismic experiments conducted in the Tricastin area (French Rhône valley) where an ancient canyon was dug and then filled with marls and sands. We estimated the ground motion amplification caused by this geological configuration using two approaches, the first one based on the analysis of earthquake recordings, the second one based on numerical simulations in 1D models.

Based on geological considerations and NHVSR measurements, we selected two sites located above the ancient canyon (BOLL and PAUL) and one site located at a nearby reference rock (ADHE). Despite the low-to-moderate seismicity context and the anthropogenic and industrialized environment, it was possible to record earthquakes providing usable frequency bands for amplification estimation around or above the fundamental resonance frequency (as deduced from NHVSR measurements). These earthquakes cover a wide range of distance (from about 100 to 1000 km) and of magnitude (from about 4 to 6.5) and therefore provide usable signals in different frequency bands. The amplification was computed at BOLL and PAUL using ADHE as reference rock site from these weak-motion earthquakes using the SSR approach. SSR curves present a plateau-like shape and reaches a value of 6 on the horizontal components (4 on the vertical component).

We also test the capacity of the seismic ambient noise to assess amplification computed from earthquake recordings at these stations. Amplification computed from SSRn and SSRh approaches at PAUL is similar to the one obtained from SSR, respectively until about 0.5 Hz (corresponding to f0) and 1 Hz.

We also carried out SWDA measurements at BOLL and ADHE to obtain local 1D Vs profiles. Vs profiles computed at BOLL show a sediment layer with a velocity of about 850 m/s and a depth estimated between 490 and 590 m. At ADHE, the experimental configuration allows us to estimate Vs30, providing a value of about 2000 m/s. At larger depth, the 1D Vs profiles show velocity slightly increasing with depth. It is worth noting that Vs profiles obtained at the two sites are consistent 1/ with the available geological data and 2/ with each other in terms of mean velocities at depth (ranging from 2800 to 3400 m/s).

Transfer functions were computed at BOLL and ADHE from these velocity profiles. The ratio of these transfer functions is computed as a numerical estimation of the ground motion amplification between BOLL and ADHE. By contrast to the empirical one, this numerical estimation shows several distinct peaks, the larger one being observed at 0.5 Hz with an amplitude of about 3-3.5. Given the

large uncertainties of this numerical amplification at high frequency, we limit our interpretation to the lower frequency part of the curve (i.e. around the fundamental resonance frequency).

Different processes are proposed to explain the discrepancies (amplitude and shape) observed around the fundamental resonance frequency between empirical and numerical amplifications. Using the Bard and Bouchon (1985) criterion, we suggest that surface waves generated at the edges of the basin play a major role.

In this study, we carried out classical and easy-to-handle seismic experiments that still allowed us to provide information about local ground motion amplifications caused by the ancient Rhône canyon. This highlights the interest of acquiring on-site observations also for areas of low-to-moderate seismicity and in industrialized and potentially noisy environments. Such measurements are preliminary. In particular, these local measurements do not allow us to catch any spatial variability of the amplification within the basin and prevent us from fully investigating processes related to the 2D/3D geometry of the basin. These perspectives are part of the French-German DARE project including a 2D/3D characterization of the basin and extended measurements at the basin scale for several months.

References

Ballesio, R. (1972). Etude stratigraphique du Pliocène rhodanien. *Doc. Lab. Géol. Fac. Sci. Lyon*, *53*(53).

Bard, P. Y., Bouchon, M. (1985). The two dimensional resonance of sediment filled valleys. *Bulletin of the Seismological Society of America, 75*, 519–541.

Bard, P.-Y., Gariel, J.-C. (1986). The seismic response of two-dimensional sedimentary deposits with large vertical velocity gradients. *Bulletin of the Seismological Society of America*, *76*(2), 343–366.

Bellier, O., Cushing, E. M., Sébrier, M. (2021). Thirty years of paleoseismic research in metropolitan France. Comptes Rendus. Géoscience, 353(S1), 339–380. https://doi.org/10.5802/crgeos.102

Bindi, D., Parolai, S., Cara, F., Di Giulio, G., Ferretti, G., Luzi, L., … Rovelli, A. (2009). Site Amplifications Observed in the Gubbio Basin, Central Italy: Hints for Lateral Propagation Effects. *Bulletin of the Seismological Society of America*, *99*(2A), 741–760. https://doi.org/10.1785/0120080238

Bitri, A., Le Bégat, S., M. Baltassat, J. (1998). Shear-waves velocity determination of soils from in-situ Rayleigh waves measurements. In *4th EEGS Meeting*. Barcelona , Spain,: European Association of Geoscientists & Engineers. https://doi.org/10.3997/2214-4609.201407156

Bodet L., 2005. Limites théoriques et expérimentales de l'interprétation de la dispersion des ondes de Rayleigh : apport de la modélisation numérique et physique. PhD thesis manuscript, 186 pp, École Centrale de Nantes et Université de Nantes

Bollinger, L., Dortz, K. L., Duverger, C., Vallage, A., Marin, S., Leroy, Y. M. (2021). Seismic swarms in Tricastin, lower Rhône Valley (France): review of historical and instrumental seismicity and models. Comptes Rendus. Géoscience, 353(S1), 585–606. https://doi.org/10.5802/crgeos.93

Bonnefoy-Claudet, S., Köhler, A., Cornou, C., Wathelet, M., Bard, P.-Y. (2008). Effects of love waves on microtremor H/V ratio. *Bulletin of the Seismological Society of America*, *98*(1), 288–300. https://doi.org/10.1785/0120070063

Borcherdt, R. D. (1970). Effects of local geology on ground motion near San Francisco Bay. *Bulletin of the Seismological Society of America*, *60*(1), 29–61. Retrieved from https://pubs.geoscienceworld.org/bssa/article-abstract/60/1/29/101559/Effects-of-local-geology-on-ground-motion-near-San

Capon, J. (1969). High-resolution frequency-wavenumber spectrum analysis. *Proceedings of the IEEE*, *57*(8), 1408–1418. https://doi.org/10.1109/PROC.1969.7278

Causse, M., Cornou, C., Maufroy, E., Grasso, J.-R., Baillet, L., El Haber, E. (2021). Exceptional ground motion during the shallow Mw 4.9 2019 Le Teil earthquake, France. Communications Earth & Environment, 2(1), 14. https://doi.org/10.1038/s43247-020-00089-Clauzon, G. (1982). (The Messinian Rhone canyon as a definite proof of the desiccated deep-basin model of Hsu, Cita and Ryan, 1973). [Le canyon messinien du Rhone: une preuve decisive du 'desiccated deep-basin model' (Hsu, Cita et Ryan 1973).]. *Bulletin, Societe Geologique de France*, *24*(3), 587–610. Retrieved from https://www.scopus.com/inward/record.uri?eid=2-s2.0-0020426611&partnerID=40&md5=d7e386fbc959a55d93fa3fe9e0a63577

Cornou, C., Ampuero, J.-P., Aubert, C., Audin, L., Baize, S., Billant, J., … Weng, H. (2021). Rapid response to the $M_{\protect \rm w}$ 4.9 earthquake of November 11, 2019 in Le Teil, Lower Rhône Valley, France. *Comptes Rendus. Géoscience*. https://doi.org/10.5802/crgeos.30

Cornou, C., Bard, P.-Y. (2003). Site-to-bedrock over 1D transfer function ratio: An indicator of the proportion of edge-generated surface waves? *Geophysical Research Letters*, *30*(9). https://doi.org/10.1029/2002GL016593

Cushing, E. M., Hollender, F., Moiriat, D., Guyonnet-Benaize, C., Theodoulidis, N., Pons-Branchu, E., … Roumelioti, Z. (2020). Building a three dimensional model of the active Plio-Quaternary basin of Argostoli (Cephalonia Island, Greece): An integrated geophysical and geological approach. *Engineering Geology*, *265*. https://doi.org/10.1016/j.enggeo.2019.105441

Delouis, B., Oral, E., Menager, M., Ampuero, J.-P., Trilla, A. G., Régnier, M., Deschamps, A. (2021). Constraining the point source parameters of the 11 November 2019 Mw 4.9 Le Teil earthquake using multiple relocation approaches, first motion and full waveform inversions. Comptes Rendus. Géoscience, 353(S1), 493–516. https://doi.org/10.5802/crgeos.78Denizot, G. (1952). Le Pliocène dans la vallée du Rhône. *Rev. Geogr. Lyon*, *27*(4), 327–357.

Denolle, M. A., Dunham, E. M., Prieto, G. A., Beroza, G. C. (2013). Ground motion prediction of realistic earthquake sources using the ambient seismic field. *Journal of Geophysical Research: Solid Earth*, *118*(5), 2102–2118. https://doi.org/10.1029/2012JB009603

El Haber, E., Cornou, C., Jongmans, D., Youssef Abdelmassih, D., Lopez-Caballero, F., AL-Bittar, T. (2019). Influence of 2D heterogeneous elastic soil properties on surface ground motion spatial variability. *Soil Dynamics and Earthquake Engineering*, *123*, 75–90. https://doi.org/10.1016/j.soildyn.2019.04.014

Felicetta, C., D'Amico, M., Lanzano, G., Puglia, R., Russo, E., Luzi, L. (2017). Site characterization of Italian accelerometric stations. *Bulletin of Earthquake Engineering*, *15*. https://doi.org/10.1007/s10518-016-9942-3

Foti, S., Comina, C., Boiero, D., Socco, L. V. (2009). Non-uniqueness in surface-wave inversion and consequences on seismic site response analyses. *Soil Dynamics and Earthquake Engineering*, *29*(6), 982–993. https://doi.org/10.1016/j.soildyn.2008.11.004

Foti F., Hollender F., Garofalo F., Albarello D., Asten M., Bard P.-Y., Comina C., Cornou C., Cox B., Di Giulio G., Forbriger T., Hayashi K., Lunedei E., Martin A., Mercerat D., Ohrnberger M., Poggi V., Renalier F., Sicilia D., Socco V.. Guidelines for the good practice of surface wave analysis: a product of the InterPACIFIC project, Bull Earthquake Eng (2018) 16:2367–2420 https://doi.org/10.1007/s10518-017-0206-7

Garofalo, F., Foti, S., Hollender, F., Bard, P. Y., Cornou, C., Cox, B. R., … Yamanaka, H. (2016). InterPACIFIC project: Comparison of invasive and non-invasive methods for seismic site characterization. Part I: Intra-comparison of surface wave methods. Soil Dynamics and Earthquake Engineering, 82, 222–240. https://doi.org/10.1016/j.soildyn.2015.12.010

Gelis, C., Leparoux, D., Virieux, J., Bitri, A., Operto, S., Grandjean, G. (2005). Numerical modeling of surface waves over shallow cavities. Journal of Environmental and Engineering Geophysics, 10(2), 111–121. https://doi.org/10.2113/JEEG10.2.111

Haskell, N. A. (1953). The dispersion of surface waves on multilayered media. Bulletin of the Seismological Society of America, 43, 17–34. Retrieved from https://pubs.geoscienceworld.org/ssa/bssa/article-abstract/43/1/17/115661/The-dispersion-of-surface-waves-on-multilayered?redirectedFrom=fulltext

Hollender, F., Cornou, C., Dechamp, A., Oghalaei, K., Renalier, F., Maufroy, E., … Sicilia, D. (2018). Characterization of site conditions (soil class, VS30, velocity profiles) for 33 stations from the French permanent accelerometric network (RAP) using surface-wave methods. Bulletin of Earthquake Engineering, 16(6), 2337–2365. https://doi.org/10.1007/s10518-017-0135-5

Ibs-von Seht, M., Wohlenberg, J. (1999). Microtremor measurements used to map thickness of soft sediments. Bulletin of the Seismological Society of America, 89(1), 250–259. https://doi.org/10.1785/BSSA0890010250

Jomard, H., Scotti, O., Auclair, S., Dominique, P., Manchuel, K., Sicilia, D. (2021). The SISFRANCE database of historical seismicity. State of the art and perspectives. Comptes Rendus - Geoscience, 353. https://doi.org/10.5802/crgeos.91

Kawase, H. (1996). The Cause of the Damage Belt in Kobe: 'The Basin-Edge Effect,' Constructive Interference of the Direct S-Wave with the Basin-Induced Diffracted/Rayleigh Waves. Seismological Research Letters, 67(5), 25–34. https://doi.org/10.1785/gssrl.67.5.25

Kennett, B. L. N., Kerry, N. J. (1979). Seismic waves in a stratified half space. Geophysical Journal International, 57(3), 557–583. https://doi.org/10.1111/j.1365-246X.1979.tb06779.x

Konno, K., Ohmachi, T. (1998). Ground-motion characteristics estimated from spectral ratio between horizontal and vertical components of microtremor. Bulletin of the Seismological Society of America, 88(1), 228–241.

Ktenidou, O.-J., Chávez-García, F.-J., Raptakis, D., Pitilakis, K. D. (2016). Directional dependence of site effects observed near a basin edge at Aegion, Greece. Bulletin of Earthquake Engineering, 14(3), 623–645. https://doi.org/10.1007/s10518-015-9843-x

Lacoss, R. T., Kelly, E. J., Toksöz, M. N. (1969). Estimation Of Seismic Noise Structure Using Arrays†. Geophysics, 34(1), 21–38. https://doi.org/10.1190/1.1439995

Lanzano, G., D'Amico, M., Felicetta, C., Puglia, R., Luzi, L., Pacor, F., Bindi, D. (2016). Ground-Motion Prediction Equations for Region-Specific Probabilistic Seismic-Hazard Analysis. Bulletin of the Seismological Society of America, 106. https://doi.org/10.1785/0120150096

Manchuel, K., Traversa, P., Baumont, D., Cara, M., Nayman, E., Durouchoux, C. (2018). The French seismic CATalogue (FCAT-17). Bulletin of Earthquake Engineering, 16(6), 2227–2251. https://doi.org/10.1007/s10518-017-0236-1

Mandier, P. (1984). Le relief de la moyenne vallée du Rhône au Tertiaire et au Quaternaire. Essai de synthèse paléogéographique. Le Relief de La Moyenne Vallée Du Rhône Au Tertiaire et Au Quaternaire.

Mascandola, C., Barani, S., Massa, M., Albarello, D. (2021). New Insights into Long-Period (>1 s) Seismic Amplification Effects in Deep Sedimentary Basins: A Case of the Po Plain Basin of Northern Italy. Bulletin of the Seismological Society of America. https://doi.org/10.1785/0120200315

Maufroy, E., Chaljub, E., Hollender, F., Bard, P.-Y., Kristek, J., Moczo, P., … Pitilakis, K. (2016). 3D numerical simulation and ground motion prediction: Verification, validation and beyond – Lessons from the E2VP project. Soil Dynamics and Earthquake Engineering, 91, 53–71. https://doi.org/10.1016/j.soildyn.2016.09.047

Michel, C., Edwards, B., Poggi, V., Burjanek, J., Roten, D., Cauzzi, C., Fah, D. (2014). Assessment of Site Effects in Alpine Regions through Systematic Site Characterization of Seismic Stations. Bulletin of the Seismological Society of America, 104(6), 2809–2826. https://doi.org/10.1785/0120140097

Mocochain, L., Audra, P., Clauzon, G., Bellier, O., Bigot, J.-Y., Parize, O., Monteil, P. (2009). The effect of river dynamics induced by the Messinian Salinity Crisis on karst landscape and caves: Example of the Lower Ardèche river (mid Rhône valley). Geomorphology, 106(1–2), 46–61. https://doi.org/10.1016/j.geomorph.2008.09.021

Mocochain, L., Clauzon, G., Bigot, J.-Y. (2006). The Ardèche endokarstic responses to the eustatic variations resulting from the Messinian salinity crisis [Réponses de l'endokarst ardéchois aux variations eustatiques générées par la crise de salinité messinienne]. Bulletin de La Societe Geologique de France, 177(1), 27–36. https://doi.org/10.2113/177.1.27

Nakamura, Y. (1989). A method for dynamic characteristics estimation of subsurface using microtremor on the ground surface. Railway Technical Research Institute, Quarterly Reports, 30(1), 25–30. Retrieved from https://trid.trb.org/view.aspx?id=294184

Park, C. B., Miller, R. D., Xia, J. (1999). Multichannel analysis of surface waves. Geophysics, 64(3), 800–808. https://doi.org/10.1190/1.1444590

Perron, V., Gélis, C., Froment, B., Hollender, F., Bard, P.-Y., Cultrera, G., Cushing, E. M. (2018). Can broad-band earthquake site responses be predicted by the ambient noise spectral ratio? Insight from observations at two sedimentary basins. Geophysical Journal International, 215(2), 1442–1454. https://doi.org/10.1093/GJI/GGY355

Perron, V., Hollender, F., Bard, P.-Y., Gélis, C., Guyonnet-Benaize, C., Hernandez, B., Ktenidou, O.-J. (2017). Robustness of kappa (κ) measurement in low-to-moderate seismicity areas: Insight from a site-specific study in provence, France. Bulletin of the Seismological Society of America, 107(5), 2272–2292. https://doi.org/10.1785/0120160374

Perron, Vincent. (2017). Contribution of seismic and ambient noise records for site-specific seismic hazard assessment in low to moderate seismicity area (PhD Thesis). Grenoble. Retrieved from http://www.theses.fr/2017GREAU020

Ritz, J.-F., Baize, S., Audin, L., Authémayou, C., Graveleau, F., Kaub, C., … Woerd, J. V. der. (2021). New perspectives in studying active faults in metropolitan France: the “Active faults France” (FACT/ATS) research axis from the Resif-Epos consortium. Comptes Rendus. Géoscience, 353(S1), 381–412. https://doi.org/10.5802/crgeos.98

Ritz, J.-F., Baize, S., Ferry, M., Larroque, C., Audin, L., Delouis, B., Mathot, E. (2020). The Mw4.9 Le Teil surface-rupturing earthquake in southern France: New insight on seismic hazard assessment in stable continental regions (other). display. https://doi.org/10.5194/egusphere-egu2020-8409

Rost, S., Thomas, C. (2002). Array Seismology: Methods and Applications. Reviews of Geophysics, 40(3), 2-1-2–27. https://doi.org/10.1029/2000RG000100

Roten, D., Fäh, D., Cornou, C., Giardini, D. (2006). Two-dimensional resonances in Alpine valleys identified from ambient vibration wavefields. Geophysical Journal International, 165(3), 889–905. https://doi.org/10.1111/j.1365-246X.2006.02935.x

Schlupp, A., Clauzon, G., Avouac, J.-P. (2001). Post Messinian movement along the Nîmes fault: Implications for the seismotectonics of Provence (France) [Mouvement post-messinien sur la faille de Nîmes: Implications pour la sismotectonique de la Provence]. Bulletin de La Societe Geologique de France, 172(6), 697–711. https://doi.org/10.2113/172.6.697

Semblat, J. F., Kham, M., Parara, E., Bard, P. Y., Pitilakis, K., Makra, K., Raptakis, D. (2005). Seismic wave amplification: Basin geometry vs soil layering. Soil Dynamics and Earthquake Engineering, 25(7–10), 529–538. https://doi.org/10.1016/j.soildyn.2004.11.003

Semblat, J.-F., Duval, A.-M., Dangla, P. (2000). Numerical analysis of seismic wave amplification in Nice (France) and comparisons with experiments. Soil Dynamics and Earthquake Engineering, 19(5), 347–362. https://doi.org/10.1016/S0267-7261(00)00016-6

SESAME team. (2004). Guidelines for the implementation of the H/V spectral ratio technique on ambient vibrations: measurements, processing and interpretation (Deliverable) (pp. 1–62). SESAME European research project.

Stokoe, K. H., II, S. G., Bay, J. A., Roesset, J. M. (1994). Characterization of geotechnical sites by SASW method, in Technical Report-Geophysical Characterization of Sites. International Conf. On Soil Mechanics and Foundation Engineering, 15–26.

Suc, J.-P., Bellier, O., Rubino, J.-L. (2011). Miocene -Pliocene geodynamics and paleogeography in the Mediterranean region: Eustasy -Tectonics interference. Bulletin de La Societe Geologique de France, 182(2), 69–71. https://doi.org/10.2113/gssgfbull.182.2.69

Tchawe, F. N., Gelis, C., Bonilla, L. F., Lopez-Caballero, F. (2021). Effects of 2-D random velocity perturbations on 2-D SH short-period ground motion simulations in the basin of Nice, France. Geophysical Journal International, 226(2), 847–861. https://doi.org/10.1093/gji/ggab141

Teague, D. P., Cox, B. R. (2016). Site response implications associated with using non-unique Vs profiles from surface wave inversion in comparison with other commonly used methods of accounting for Vs uncertainty. Soil Dynamics and Earthquake Engineering, 91, 87–103. https://doi.org/10.1016/j.soildyn.2016.07.028

Theodulidis, N., Bard, P.-Y., Archuleta, R., Bouchon, M. (1996). Horizontal-to-vertical spectral ratio and geological conditions: The case of Garner Valley Downhole Array in southern California. Bulletin of the Seismological Society of America, 86(2), 306–319. Retrieved from https://www.scopus.com/inward/record.uri?eid=2-s2.0-0030477595&partnerID=40&md5=caa4bd8780db89cff7a30b6f94e1348b

Thompson, E. M., Baise, L. G., Kayen, R. E., Guzina, B. B. (2009). Impediments to Predicting Site Response: Seismic Property Estimation and Modeling Simplifications. Bulletin of the Seismological Society of America, 99(5), 2927–2949. https://doi.org/10.1785/0120080224

Thompson, W. T. (1950). Transmission of Elastic Waves through a Stratified Solid Medium. Journal of Applied Physics, 21(2), 89–93. https://doi.org/10.1063/1.1699629

Thouvenot, F., Jenatton, L., Gratier, J.-P. (2009). 200-m-deep earthquake swarm in Tricastin (lower Rhône Valley, France) accounts for noisy seismicity over past centuries. Terra Nova, 21(3), 203–210. https://doi.org/10.1111/j.1365-3121.2009.00875.x

Toro, G. R. (1995). Probabilistic models of the site velocity profiles for generic and site- specific ground-motion amplification studies. (Technical Report No. 77957) (p. 147). Upton, N.Y.: Brookhaven National Laboratory.

Vallage, A., Bollinger, L., Champenois, J., Duverger, C., Trilla, A. G., Hernandez, B., … Vergoz, J. (2021). Multitechnology characterization of an unusual surface rupturing intraplate earthquake: the ML 5.4 2019 Le Teil event in France. Geophysical Journal International, 226(2), 803–813. https://doi.org/10.1093/gji/ggab136

Wathelet, M. (2008). An improved neighborhood algorithm: Parameter conditions and dynamic scaling. Geophysical Research Letters, 35(9). https://doi.org/10.1029/2008GL033256

Wathelet, Marc, Chatelain, J.-L., Cornou, C., Giulio, G. D., Guillier, B., Ohrnberger, M., Savvaidis, A. (2020). Geopsy: A User-Friendly Open-Source Tool Set for Ambient Vibration Processing. Seismological Research Letters, 91(3), 1878–1889. https://doi.org/10.1785/0220190360

Acknowledgments

We warmly thank landowners and city halls to let us install our stations at BOLL, PAUL and ADHE. We greatly thank F. Hollender (CEA) for having lendt us his MASW acquisition and A. Bitri (BRGM) for having let us using his MASW processing code. This study was founded from IRSN's own resources.

We are very grateful to the two reviewers and the associate editor for their constructive comments and suggestions to improve the manuscript.

This publication is dedicated to the memory of our colleague and friend Christophe Clément.

Declarations

Funding : this research was supported by IRSN

Conflicts of interest/Competing interests (include appropriate disclosures) : Not applicable

Availability of data and material (data transparency) : Seismic records are available upon request

Code availability (software application or custom code) : Geopsy used for HVSR and AVA processing is an open-source software ; Code used for SSR computation is a custom code.